

# Geochemistry of basement rocks from SE Kenya and NE Tanzania: indications for rifting and early Pan-African subduction

A. H. Bauernhofer · C. A. Hauzenberger ·  
E. Wallbrecher · S. Muhongo · G. Hoinkes ·  
A. Mogessie · N. Opiyo-Akech · V. Tenczer

Received: 28 July 2006 / Accepted: 23 June 2008 / Published online: 19 July 2008  
© Springer-Verlag 2008

**Abstract** Amphibolites and orthogneisses from the Taita Hills-Galana River area (SE Kenya) indicate their broad geological-tectonic setting. There are groups of subduction-related rocks which show characteristic REE (rare earth element) patterns and enrichment or varying concentrations of HFS (high field strength) elements. The groups can be assigned to tectonostratigraphic domains marked by different structural styles (e.g., thrust- or strike-slip dominated). Tholeiitic gneisses, often emerging as folded and isolated (ridge-shaped) leucocratic bodies, belong to a group of rocks located between the thrust- and strike-slip domain. Compared to calc-alkaline gneisses of the area they contain more mafic inclusions and have lower LIL (large ionic lithophile), HFS and light REE values. These gneisses have chemical characteristics of M-type granitoids of oceanic island arc signature. Intrusion ages of ~955–845 Ma determined for these rocks suggest early Pan-African subduction. Mafic to ultramafic rocks from the Pare mountains of NE Tanzania show evidence of ophiolitic cumulates, subduction settings were also observed for the granulite areas in central and southern Tanzania. Together with the widespread arc settings documented in the Arabian–Nubian Shield, the presented data supports the

continuation of an island-continental arc range across Kenya–Tanzania to Mozambique.

**Keywords** Rifting · Subduction · Volcanic arcs · Pan-African convergence · Mozambique belt

## Introduction

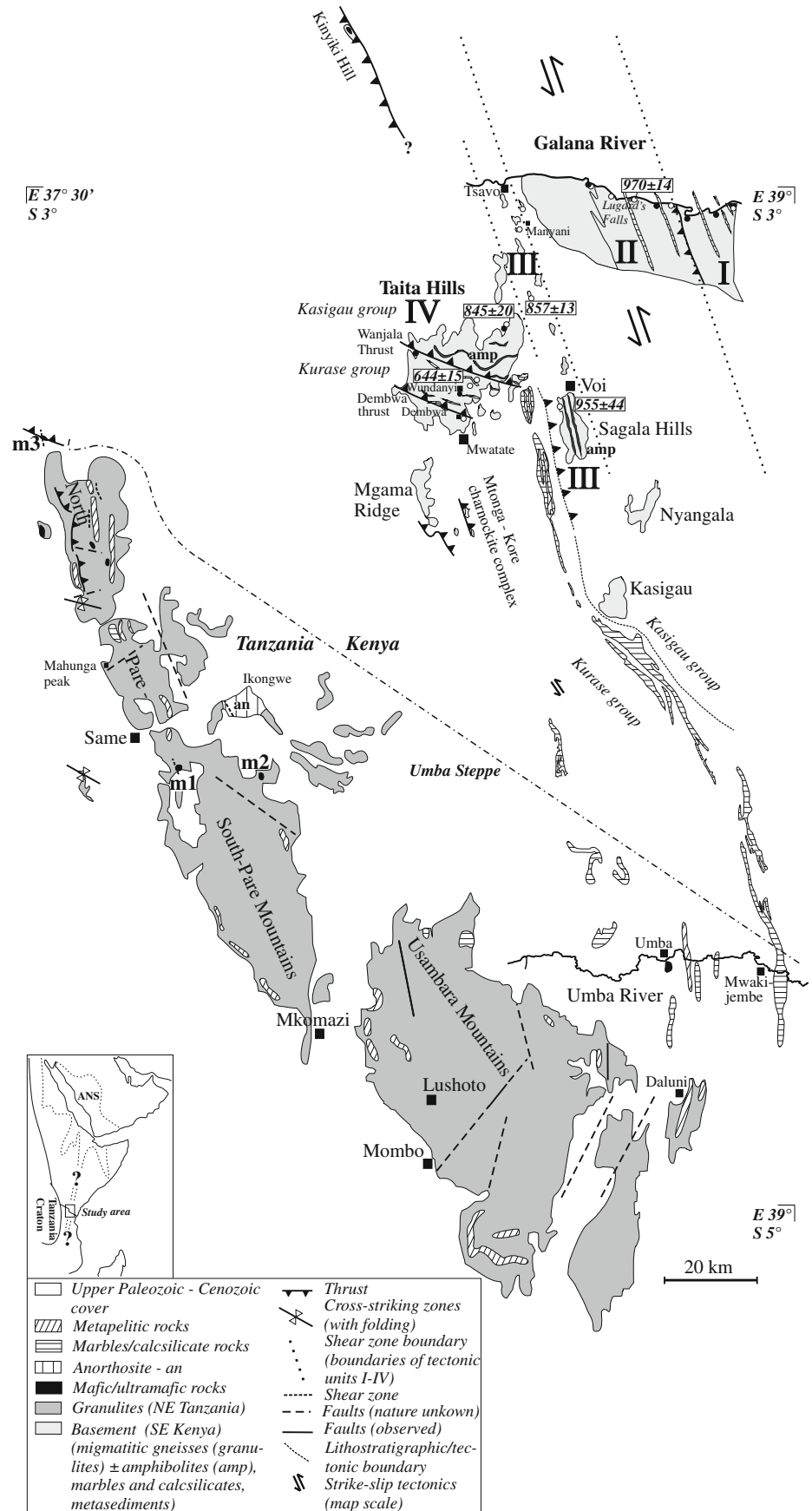
The Taita Hills-Galana River area near Voi in SE Kenya and the Pare-Usambara mountains in NE Tanzania (Figs. 1, 12) belong to the easternmost basement areas in the Mozambique Belt of East Africa. Many studies document high grade metamorphic conditions for rocks of Kenya and Tanzania (e.g., Coolen et al. 1982; Pohl et al. 1980; Key et al. 1989; Appel et al. 1998; Möller et al. 2000; Muhongo et al. 2001; Johnson et al. 2003; Sommer et al. 2003; Kröner et al. 2003; Hauzenberger et al. 2004; Tenczer et al. 2006). These rocks forming the root of the mountains comprise a variety of metasedimentary and metamagmatic rocks. Several sites of ophiolitic rocks are documented in northern Kenya. There is evidence (e.g., Berhe 1990) for rocks of a supra-subduction zone (Baragoi) or a back-arc environment (Moyale). In SE Kenya, Frisch and Pohl (1986) indicated ophiolitic remnants, subduction and rift related mafic rocks (Voi suture zone) at Kinyiki Hill and in the Taita Hills (Fig. 1). In the same region, several types of ultrabasic rocks associated with gem corundum mineralization have been distinguished (Mercier et al. 1999). They were formed under granulite facies conditions and appear to be tectonically emplaced bodies within the surrounding country rocks. The neighbouring Pare-Usambara mountains and the Uмба Steppe area in NE Tanzania also contain various mafic- to ultra-mafic rocks which usually occur as small, isolated bodies. To some extent, they could

A. H. Bauernhofer (✉) · C. A. Hauzenberger · E. Wallbrecher ·  
G. Hoinkes · A. Mogessie · V. Tenczer  
Institute for Earth Sciences, University of Graz,  
Heinrichstraße 26, 8010 Graz, Austria  
e-mail: andreas.bauernhofer@uni-graz.at

S. Muhongo  
Department of Geology, University of Dar es Salaam,  
P.O. Box 35052, Dar es Salaam, Tanzania

N. Opiyo-Akech  
Department of Geology, University of Nairobi,  
P.O. Box 30197, Nairobi, Kenya

**Fig. 1** Study area in SE Kenya and NE Tanzania. Redrawn (including some structural data) after Saggerson (1962), Sanders (1963), Pohl and Niedermayr (1979), Horkel et al. (1979), Bagnall (1960), Dundas (1965), Bagnall et al. (1963), Hartley and Moore (1965), and Möller et al. (2000). Not all isolated outcrops of the study area are shown. Boundary of Kurase-Kasigau group from Saggerson (1962) and Pohl et al. (1980). Indices I–IV, tectonostratigraphic units (SE Kenya). *Filled* (amphibolite)- and *open* (gneiss) circles indicate sample locations in SE Kenya, m1–m3 mark outcrops in the Pare Mountains. The Voi suture zone (Frisch and Pohl 1986) extends along the lithotectonic boundary of the Kurase- and Kasigau group. Indicated (emplacement) ages of gneisses from Hauzenberger et al. (2007). *Inset* shows the study area (rectangle at the Kenya/Tanzania border) in relation to the Arabian–Nubian Shield (dotted curve outlines the approximate domain of Pan-African volcanic arc rocks)



represent the continuation of the SE Kenyan zone. This is supported by geochemical data of metagranitoids (Appel 1996; Maboko and Nakamura 2002) which indicate a convergent arc setting for NE Tanzania.

New geochemical data from SE Kenya and NE Tanzania are shown in Table 1. In addition, we present published geochemical data of the Voi suture zone (Frisch and Pohl 1986), NE Tanzania (Maboko and Nakamura 2002) and SE Tanzania (Kröner et al. 2003) in discrimination diagrams. Most of the previous age data from SE Tanzania indicate younger igneous ages ( $\sim 800$ – $632$  Ma) compared to those detected in the study area ( $\sim 970$ – $845$  Ma). Considering both geochemical results and recent igneous ages, we attempt to address questions of character and tectonic style of the East African Mozambique Belt, as well as the timing of Pan-African events. The term “Pan-African” is used here in a broad sense for the Neoproterozoic inasmuch age datings from the study area relate to events almost covering the entire era. The geochemical data are from a variety of metaigneous (ultramafic to acidic) rocks which can be found along a  $\sim 150$  km E-W cross section characterized by a conspicuous change in the tectonic style (Figs. 1, 12). A main effort of this work is to determine possible tectonic setting(s) for these rocks.

## Regional geology

### Mozambique belt

The Mozambique orogenic belt in Kenya and Tanzania (e.g., Shackleton 1986) consists of metasediments, marbles, calc-silicate rocks, migmatites, gneisses and metaigneous- to metasedimentary granulites. In addition, mafic- to ultramafic rocks, mafic gneisses, massive-type meta-anorthosites as well as tectonized- and post-kinematic granites are present. These lithologies, often highly deformed and metamorphosed during Pan-African tectonothermal events ( $<900$  to  $\leq 500$  Ma), include reworked Archean- to Mesoproterozoic basement (frequently exposed, e.g., in the more western part of the belt; Fig. 12) and additions of newly formed Neoproterozoic crust, as can be found in SE Kenya and NE Tanzania.

### SE Kenya

The Taita Hills area near Voi (Fig. 1), at first divided into arenaceous and argillaceous lithologies (Parkinson 1947), form a S-SW directed tectonically imbricated nappe stack which shallowly dips to the NNE. Horkel et al. (1979) and Pohl et al. (1980) differentiated a lower Kurase- and overlying Kasigau group which were also documented in the SE (Fig. 1) by Saggerson (1962). The Kurase group

contains metasediments (quartzites, graphite and kyanite to sillimanite gneisses), marbles and amphibolites are interpreted to represent a rifted shelf sequence. Granulitic to charnockitic slices are found sporadically and could represent reworked basement of the group (Pohl et al. 1980). Quartz–feldspar–biotite–hornblende gneisses and intercalated amphibolites (thought to be subduction derived) are abundant in the Kasigau group. These rocks are associated with continental margin sediments. Amphibolites, serpentinites and pyroxene-talc-amphibole rocks (e.g., Farquhar 1960) often occurring at the thrust contact of the groups (Wanjala thrust; Pohl et al. 1980; Fig. 1) were interpreted as tectonized vestiges of oceanic crust (Voi suture zone; Frisch and Pohl 1986).

The deformational history of the Taita Hills comprises three folding events (F1–F3, Horkel et al. 1979; Pohl et al. 1980). The earliest deformation (D1/F1) caused tight to isoclinal and westward overturned folds (NNW plunging axes). In addition, ophiolitic rocks were arranged along thrusts. The same style of folding but about NNE plunging axes was associated with the subsequent deformation (D2/F2). Related small-scale structures are, e.g., shear folds, cross folds (sporadically) and fold interference patterns. The contemporaneous metamorphism resulted in migmatization of the rocks. A late deformation event (D3/F3) produced large open folds and gentle flexures with the axes trending north.

The eastern portion of the Galana River area (Sanders 1963; Fig. 1) is overlain by the upper Paleozoic Duruma sandstones. These include arkoses, sandstones, shales and limestones and show a fault contact to the subjacent basement, the Precambrian Sobo formation (Sanders 1963). The Precambrian rocks were metamorphosed under granulite- to amphibolite facies conditions. The common rocks are garnetiferous schists and granulites, thin quartzites, coarse grained marbles, hornblende gneisses and garnet amphibolites. Foliations often dip either gently (up to  $20^\circ$ ) to the NW or moderately ( $\sim 40^\circ$ ) to the SE.

Towards the west, steep westerly dipping rocks occur. The sequence (Lugard’s Falls belt; Sanders 1963; Fig. 1) shows banded migmatitic biotite-hornblende gneisses and contain pegmatitic segregations. Intercalated are migmatized garnet and diopside bearing gneisses and to a minor extent marbles. Structural observations indicate flattening geometry and large scale strike slip tectonics (Bauernhofer 2003). The western continuation of the zone (Sanders 1963) includes isoclinally folded garnet and graphite bearing gneisses with thin strips of hornblende and hornblende-garnet gneisses. At the Sagala Hills (Fig. 1), the gneisses often contain diopside-rich lenses and “schlieren” (Sanders 1963).

All of these domains show different tectonic styles and lithologic variations. Hence, four tectonostratigraphic units

**Table 1** Geochemical analyses of rocks of the study area

Tect. unit	m1					m2					m3		
Lat. (S)	04°08'16''					04°08'56''					03°26'58''		
Long. (E)	37°48'48''					37°58'08''					37°32'06''		
Rock Type	px-hbl-gnr.	hbl-gnr.	pl-hbl-pxn.	px-hbl-gnr.	hbl-gbr.	spl-hbl-gbr.	amr/mfgr.	hbl-gbr.	hbl-gbr.	amr/mfgr.	spl-cpxn.	gbr.	
Sample	147-1	147-2	147-3	147-4	147-5	149-1	149-2	149-3	149-4	152-0	152-1	152-2	
SiO <sub>2</sub>	43.61	45.46	40.58	42.35	49.25	36.73	37.47	38.11	39.28	41.73	46.83	47.79	
Al <sub>2</sub> O <sub>3</sub>	16.38	16.85	23.65	12.01	21.11	15.96	14.44	13.75	17.36	15.93	12.73	13.83	
Fe <sub>2</sub> O <sub>3</sub>	10.47	9.21	9.71	11.17	7.01	19.87	19.61	17.58	16.99	15.16	5.26	3.48	
MnO	0.16	0.17	0.25	0.20	0.17	0.29	0.32	0.28	0.26	0.23	0.11	0.11	
MgO	12.21	12.11	3.83	11.09	3.26	8.98	6.09	8.20	7.84	8.36	16.97	10.39	
CaO	12.59	12.90	19.54	20.67	12.00	14.48	12.87	12.52	12.97	13.87	16.44	22.10	
Na <sub>2</sub> O	2.10	1.78	0.62	0.71	3.96	1.60	1.41	1.93	1.70	1.59	0.64	0.36	
K <sub>2</sub> O	0.38	0.44	0.17	0.14	0.37	0.26	0.83	0.86	0.67	0.28	0.10	0.22	
TiO <sub>2</sub>	0.29	0.07	0.70	0.26	0.60	1.03	4.13	4.18	0.91	1.28	0.09	0.09	
P <sub>2</sub> O <sub>5</sub>	0.02	0.02	0.04	0.01	0.21	0.10	0.41	0.70	0.08	0.12	<0.01	0.03	
LOI	1.40	1.23	0.34	1.50	0.44	0.62	-0.01	0.34	0.54	0.02	1.31	0.49	
Total	99.60	100.24	99.42	100.11	98.38	99.92	97.59	98.45	98.59	98.57	100.48	98.88	
Mg/(Mg + Fe)	0.70	0.72	0.44	0.66	0.48	0.47	0.38	0.48	0.48	0.52	0.86	0.86	
Sc	34	59	22	63	20	72	49	34	59	57	41	53	
Be	<1	<1	<1	<1	1	<1	1	2	<1	<1	<1	<1	
V	399	268	126	270	100	488	563	332	434	360	116	125	
Cr	24	90	<20	492	<20	63	64	445	62	316	789	247	
CO	80.9	62.5	19.8	65.1	16.5	70.6	58	69.7	59.6	84.3	64.3	27.8	
Ni	42	61.5	<20	103.2	<20	52.7	82.5	807.7	57.8	131.5	296.1	94.3	
Cu	18	13	<10	14	<10	13	18	11	11	25	24	16	
Zn	<30	<30	<30	61	44	75	<30	123	47	36	35	<30	
Ga	12.69	6.04	17.87	11.54	16.58	8.70	16.73	24.25	13.01	18.24	7.30	6.70	
Li	1.30	1.41	0.60	2.52	0.59	<0.5	0.61	1.24	0.73	1.69	1.05	0.73	
Rb	2.10	6.75	4.61	3.64	3.32	2.82	7.35	5.34	8.4	2.28	2.21	4.72	
Sr	210	272	2260	364	1090	465	378	484	893	166	43	73.9	
Y	1.5	1.1	38.9	6	28	30.5	61.7	38.8	26.6	28.2	3.7	2.8	
Zr	13.1	11.6	178.6	13.5	149.2	43.2	144.9	293.6	33.3	61.1	2.9	12.5	
Nb	0.35	0.29	7.67	0.71	10.31	0.50	12.18	53.18	1.47	3.18	0.25	0.44	
Cs	<0.1	0.27	0.12	1.12	0.23	<0.1	<0.1	<0.1	<0.1	0.16	<0.1	<0.1	
Ba	42.9	36.7	664	56.6	1200	196	386	241	700	72.7	18.1	147	
La	0.93	0.98	31.1	2.49	20.4	2.2	20.1	51.1	2.27	4.87	0.54	0.63	
Ce	1.59	1.25	58.34	6.52	42.21	6.01	49.01	107.9	5.75	12.88	1	0.96	
Pr	0.18	0.11	6.79	0.79	4.43	0.89	6.12	11.1	0.81	1.65	0.15	0.11	
Nd	0.76	0.42	28.14	3.72	19.61	5.64	30.11	51.23	4.79	8.48	0.73	0.51	
Sm	0.16	0.10	5.99	0.95	4.36	2.37	8.42	10.81	1.93	2.85	0.32	0.22	
Eu	0.17	0.12	1.67	0.21	1.33	0.97	3.48	3.79	0.83	1.13	0.19	0.12	
Gd	0.22	0.13	5.63	0.97	4.46	3.30	10.27	9.34	2.97	3.65	0.42	0.32	
Tb	0.03	0.02	1.02	0.16	0.72	0.70	1.72	1.40	0.58	0.67	0.09	0.06	
Dy	0.24	0.18	5.91	1.03	4.36	4.93	10.50	7.83	4.06	4.44	0.66	0.48	
Ho	0.05	0.04	1.20	0.21	0.91	1.08	2.14	1.39	0.92	0.98	0.14	0.10	
Er	0.16	0.14	4.19	0.67	2.93	3.42	6.34	3.73	2.86	3.01	0.43	0.31	
Tm	0.02	0.02	0.69	0.11	0.49	0.57	0.95	0.53	0.46	0.48	0.06	0.04	
Yb	0.18	0.15	4.56	0.74	3.12	3.55	5.75	3.14	2.96	3.12	0.40	0.30	
Lu	0.03	0.02	0.72	0.10	0.49	0.53	0.86	0.40	0.47	0.50	0.06	0.04	

**Table 1** continued

Tect. unit	m1					m2				m3		
Lat. (S)	04°08'16"					04°08'56"				03°26'58"		
Long. (E)	37°48'48"					37°58'08"				37°32'06"		
Rock Type	px-hbl-gnr.	hbl-gnr.	pl-hbl-pxn.	px-hbl-gnr.	hbl-gbr.	spl-hbl-gbr.	amr/mfgr.	hbl-gbr.	hbl-gbr.	amr/mfgr.	spl-cpxn.	gbr.
Sample	147-1	147-2	147-3	147-4	147-5	149-1	149-2	149-3	149-4	152-0	152-1	152-2
Hf	<0.1	<0.1	5.16	0.14	4.01	1.38	4.27	7.70	1.15	1.69	<0.1	0.12
Pb	<5	<5	<5	8.08	14.1	<5	<5	<5	<5	<5	5.55	<5
Th	0.17	0.38	5.07	0.33	3.45	0.15	1.95	5.52	0.21	0.49	0.10	0.27
U	0.07	0.14	0.90	0.09	1.18	0.07	0.88	1.43	0.08	0.12	0.05	0.09
Tect. unit	am I										am II	
Lat. (S)	03°02'50"					03°02'38"					03°03'01"	
Long. (E)	38°54'25"					38°53'59"					38°45'06"	
Rock Type	amr.					amr.					gt-amr.	
Sample	A14					F2					K57	
SiO <sub>2</sub>	46.33					54.54					46.26	
Al <sub>2</sub> O <sub>3</sub>	13.28					16.49					13.64	
Fe <sub>2</sub> O <sub>3</sub>	15.45					7.79					14.08	
MnO	0.28					0.17					0.21	
MgO	5.37					5.55					7.94	
CaO	8.80					7.83					11.99	
Na <sub>2</sub> O	2.96					4.68					2.20	
K <sub>2</sub> O	1.74					1.32					0.52	
TiO <sub>2</sub>	2.98					0.70					1.15	
P <sub>2</sub> O <sub>5</sub>	0.63					0.18					0.03	
LOI	0.87					1.58					0.83	
Total	98.69					100.83					98.85	
Mg/(Mg + Fe)	0.41					0.59					0.53	
Sc	51					25					50	
Be	1					<1					<1	
V	361					169					332	
Cr	65					130					241	
CO	48.4					64.8					65.6	
Ni	38.1					37.7					97.2	
Cu	44					<10					66	
Zn	125					75					62	
Ga	18.43					17.28					15.82	
Li	0.87					1.49					1.22	
Rb	35.54					22.27					9.19	
Sr	256					645					119	
Y	53.1					13.7					23.2	
Zr	166.1					66.2					28.7	
Nb	5.18					2.22					0.55	
Cs	0.37					0.19					0.16	
Ba	994					615					307	
La	13.9					13.4					5.06	
Ce	37.65					29.71					9.56	
Pr	5.32					3.58					1.07	
Nd	28.86					15.36					5.51	

**Table 1** continued

Tect. unit	am I					am II
Lat. (S)	03°02'50''	03°02'38''	03°03'08''	03°04'21''	03°03'01''	03°03'01''
Long. (E)	38°54'25''	38°53'59''	38°51'52''	38°48'22''	38°45'06''	38°45'06''
Rock Type	amr.	amr.	amr.	gt-amr.	gt-amr.	gt-amr.
Sample	A14	F2	KTB98	K57	K57	KGB27
Sm	8.31	3.27	6.72	7.55	7.55	2.18
Eu	2.97	1.29	2.22	2.76	2.76	0.97
Gd	9.67	2.92	7.94	8.95	8.95	3.16
Tb	1.58	0.43	1.35	1.71	1.71	0.61
Dy	9.60	2.56	8.53	10.76	10.76	4.03
Ho	1.94	0.48	1.80	2.13	2.13	0.88
Er	5.75	1.46	5.45	6.81	6.81	2.66
Tm	0.81	0.19	0.82	1.03	1.03	0.42
Yb	4.84	1.32	5.11	6.85	6.85	2.55
Lu	0.70	0.20	0.75	1.00	1.00	0.38
Hf	4.49	1.96	4.67	6.67	6.67	0.95
Pb	<5	7.95	<5	7.54	7.54	8.38
Th	0.68	1.21	1.30	1.85	1.85	0.68
U	0.40	0.41	0.54	0.67	0.67	0.55

Tect. unit	am II			am IV			gn I	gn II			
Lat. (S)	03°00'30''			03°17'02''	03°19'07''	03°24'35''	03°02'43''	03°03'03''	03°02'28''	03°02'00''	03°00'50''
Long. (E)	38°36'30''			38°26'20''	38°16'19''	38°21'45''	38°53'17''	38°46'42''	38°41'46''	38°23'05''	38°37'02''
Rock type	amr.	gt-amr.	amr.	amr.	gt-amr.	amr.	gt-bt-gn.	bt-hbl-gn.	bt-hbl-gn.	bt-hbl-gn.	bt-hbl-gn.
Sample	KGB173	K108	KGB49 A	AKTB55	KTB175	KTB60	K13	MB153	KGB35LF	KGB170	KGB49C
SiO <sub>2</sub>	46.54	46.61	43.26	49.39	53.69	43.83	61.52	58.56	62.77	63.26	59.05
Al <sub>2</sub> O <sub>3</sub>	9.19	11.33	14.66	15.58	15.86	14.87	17.08	17.22	15.59	16.38	16.75
Fe <sub>2</sub> O <sub>3</sub>	10.93	10.97	12.73	14.53	9.67	16.09	7.55	6.14	5.29	5.44	7.00
MnO	0.19	0.19	0.20	0.20	0.13	0.22	0.17	0.11	0.08	0.09	0.11
MgO	14.85	13.20	8.90	5.81	6.32	6.58	1.87	3.38	2.41	2.04	3.64
CaO	16.03	15.01	13.64	9.51	9.33	7.13	4.18	6.35	4.46	5.10	6.11
Na <sub>2</sub> O	0.87	0.89	1.88	3.04	2.48	2.65	3.83	4.81	3.97	4.60	3.96
K <sub>2</sub> O	0.17	0.59	0.85	0.48	0.47	3.19	2.21	1.38	2.76	1.69	1.79
TiO <sub>2</sub>	0.75	0.68	1.10	1.29	1.39	3.56	1.21	0.68	0.58	0.84	0.98
P <sub>2</sub> O <sub>5</sub>	0.09	0.06	0.09	0.18	0.26	0.65	0.36	0.33	0.23	0.19	0.35
LOI	0.64	0.77	0.91	0.84	0.53	1.26	0.95	0.83	0.89	0.46	0.93
Total	100.25	100.30	98.22	100.85	100.13	100.03	100.93	99.79	99.03	100.09	100.67
Mg/(Mg + Fe)	0.73	0.70	0.58	0.44	0.56	0.45					
A/CNK							1.05	0.82	0.88	0.88	0.86
Sc	82	66	52	38	22	20	20	13	12	13	15
Be	<1	<1	<1	<1	1	2	1	2	2	2	2
V	253	251	414	355	165	245	121	103	89.9	100	138
Cr	716	491	82	44.2	301	29.1	41.1	63.1	41.3	22.1	115
CO	76.7	78.9	60	88.6	80.4	58.3	56.9	39.2	62.3	53.6	86.1
Ni	158	129.8	61.9	69.2	179.6	79.5	25.9	30.4	19.1	<20	58.4
Cu	43	27	10	40	56	22	66	12	<10	41	50
Zn	<30	<30	<30	106	<30	174	160	<30	66	<30	95
Ga	10.58	7.00	16.35	19.25	13.94	20.94	20.96	17.92	18.67	15.30	22.40
Li	1.76	<0.5	1.37	1.53	<0.5	1.46	1.34	0.82	1.08	0.86	1.30

**Table 1** continued

Tect. unit	am II			am IV			gn I	gn II			
Lat. (S)	03°00'30"			03°17'02"	03°19'07"	03°24'35"	03°02'43"	03°03'03"	03°02'28"	03°02'00"	03°00'50"
Long. (E)	38°36'30"			38°26'20"	38°16'19"	38°21'45"	38°53'17"	38°46'42"	38°41'46"	38°23'05"	38°37'02"
Rock type	amr.	gt-amr.	amr.	amr.	gt-amr.	amr.	gt-bt-gn.	bt-hbl-gn.	bt-hbl-gn.	bt-hbl-gn.	bt-hbl-gn.
Sample	KGB173	K108	KGB49 A	AKTB55	KTB175	KTB60	K13	MB153	KGB35LF	KGB170	KGB49C
Rb	4.86	14.13	19.24	5.07	2.46	53.24	55.15	26.77	87.27	35.65	77.94
Sr	351	389	479	228	766	500	369	1050	860	619	785
Y	15.9	15.1	15.4	31.3	12.2	29.4	37.9	17	15	22.4	19.8
Zr	30.9	30.5	24.2	85.4	65	215.8	245.9	151.1	179.43	197.5	205.2
Nb	0.88	1.05	1.15	2.51	8.58	28.94	10.46	8.29	7.77	6.45	5.95
Cs	<0.1	0.26	0.11	<0.1	<0.1	1.57	1.08	0.29	1.17	1.07	1.60
Ba	98.9	134	129	154	91.3	708	511	838	1450	509	647
La	3.92	3.48	4.75	5.20	8.47	22.94	28.33	39.22	36.05	27.69	24.21
Ce	10.05	9.34	12.21	11.43	22.59	56.16	62.92	78.31	64.91	59.51	53.47
Pr	1.65	1.36	1.67	2.18	2.91	7.91	7.37	8.20	7.04	6.50	6.36
Nd	9.64	7.84	9.17	11.44	14.39	31.39	30.37	33.83	24.40	27.24	26.22
Sm	3.01	2.53	2.84	3.37	3.54	6.45	6.34	5.91	4.12	5.79	5.16
Eu	1.02	0.87	1.17	1.44	1.50	2.83	2.02	1.85	1.13	1.48	1.70
Gd	3.27	2.70	3.01	4.24	0.21	5.83	6.26	4.59	3.24	4.96	4.69
Tb	0.51	0.46	0.48	0.83	0.46	0.94	1.07	0.57	0.45	0.73	0.70
Dy	2.94	2.68	2.88	5.28	2.55	5.09	6.47	3.11	2.44	4.22	3.70
Ho	0.56	0.52	0.55	1.06	0.46	0.99	1.28	0.58	0.49	0.82	0.67
Er	1.61	1.51	1.58	3.38	1.22	2.77	4.13	1.64	1.41	2.34	2.03
Tm	0.23	0.23	0.24	0.48	0.16	0.36	0.63	0.23	0.19	0.34	0.26
Yb	1.40	1.35	1.48	3.19	0.94	2.31	3.82	1.42	1.25	2.11	1.70
Lu	0.19	0.18	0.20	0.47	0.12	0.34	0.59	0.20	0.18	0.29	0.25
Hf	1.12	1.00	0.75	2.41	1.93	4.89	6.34	3.70	4.82	6.04	5.31
Pb	<5	<5	<5	<5	<5	9.10	11.34	<5	19.06	<5	12.85
Th	0.24	0.41	0.35	0.44	0.67	1.70	4.03	1.05	14.05	10.37	3.48
U	0.29	0.22	1.54	0.38	0.52	1.65	0.88	0.44	1.85	0.53	1.44

Tect. unit	gn III				gn IV				
Lat. (S)	03°02'14"	03°26'53"	03°13'34"	03°05'55"	03°17'06"	03°23'14"	03°23'52"	03°27'01"	
Long. (E)	38°29'45"	38°33'40"	38°29'53"	38°28'09"	38°26'05"	38°23'25"	38°23'23"	38°21'45"	
Rock type	gt-bt-hbl-gn.	gt-hbl-gn.	gt-bt-hbl-gn.	gt-cpx-hbl-gn.	gt-bt-hbl-gn.	gt-bt-gn.	hbl-bt-gn.	bt-hbl-gn.	
Sample	K115	K209	KGB174	K154	K120	K37	KTB46A	MDB	
SiO <sub>2</sub>	66.53	67.43	63.07	73.94	75.84	65.82	68.34	62.26	
Al <sub>2</sub> O <sub>3</sub>	14.98	14.66	15.94	13.04	12.25	17.90	14.95	16.36	
Fe <sub>2</sub> O <sub>3</sub>	7.95	6.31	6.76	5.03	3.89	3.92	3.36	5.82	
MnO	0.17	0.14	0.11	0.14	0.09	0.05	0.06	0.08	
MgO	1.32	1.40	2.75	0.56	0.55	1.10	0.86	2.86	
CaO	5.42	5.64	5.67	3.56	3.47	3.20	2.42	4.83	
Na <sub>2</sub> O	3.19	3.22	3.65	3.91	3.46	4.81	3.87	4.30	
K <sub>2</sub> O	0.66	0.32	1.32	0.24	0.57	2.74	4.24	1.76	
TiO <sub>2</sub>	0.37	0.35	0.80	0.23	0.22	0.68	0.58	0.92	
P <sub>2</sub> O <sub>5</sub>	0.14	0.10	0.18	0.08	0.08	0.20	0.15	0.19	
LOI	0.05	-0.07	0.41	-0.04	0.22	0.41	0.41	0.95	
Total	100.78	99.57	100.66	100.73	100.64	100.83	99.24	100.33	
Mg/(Mg + Fe)									

**Table 1** continued

Tect. unit	gn III					gn IV		
	03°02'14"	03°26'53"	03°13'34"	03°05'55"	03°17'06"	03°23'14"	03°23'52"	03°27'01"
Lat. (S)	03°02'14"	03°26'53"	03°13'34"	03°05'55"	03°17'06"	03°23'14"	03°23'52"	03°27'01"
Long. (E)	38°29'45"	38°33'40"	38°29'53"	38°28'09"	38°26'05"	38°23'25"	38°23'23"	38°21'45"
Rock type	gt-bt-hbl-gn.	gt-hbl-gn.	gt-bt-hbl-gn.	gt-cpx-hbl-gn.	gt-bt-hbl-gn.	gt-bt-gn.	hbl-bt-gn.	bt-hbl-gn.
Sample	K115	K209	KGB174	K154	K120	K37	KTB46A	MDB
A/CNK	0.95	0.92	0.90	0.99	0.97	1.07	0.97	0.92
Sc	29	22	18	17	17	6	7	14
Be	<1	<1	1	<1	<1	2	2	1
V	56.6	66.9	84.3	17.9	25.5	43	31.7	94.1
Cr	<20	<20	30.9	<20	<20	<20	<20	34.9
CO	85.2	84.1	80.6	74	99	78.5	42	88.5
Ni	<15	<15	<20	<15	<15	<15	<20	28.4
Cu	98	<10	14	<10	<10	<10	<10	11
Zn	109	77	<30	55	43	49	30	88
Ga	17.33	14.10	17.87	16.45	12.86	22.55	17.78	20.41
Li	1.64	1.46	0.93	1.54	1.21	0.84	0.62	1.14
Rb	4.60	<2	48.39	<2	8.83	58.55	74.28	49.59
Sr	384	122	296	166	118	397	269	443
Y	16.4	23.2	23.7	46	36	13.1	25.4	19.5
Zr	24.5	40.4	95.4	85.4	91.6	352.9	342.09	235.6
Nb	1.78	1.39	4.35	1.21	1.80	11.12	14.59	4.80
Cs	<0.1	<0.1	1.47	<0.1	<0.1	1.43	0.78	1.00
Ba	220	69.1	415	111	278	835	927	610
La	2.88	2.78	11.78	6.65	8.64	41.70	57.72	41.88
Ce	7.19	7.63	26.53	14.64	18.57	80.77	106.31	86.60
Pr	1.05	1.18	3.07	2.22	2.61	8.47	9.58	8.42
Nd	5.45	6.21	13.60	11.14	12.44	30.46	35.61	30.17
Sm	2.03	2.10	3.57	3.39	3.41	5.13	6.50	4.86
Eu	1.09	0.83	1.07	0.91	0.84	1.56	1.34	1.53
Gd	2.60	2.70	3.72	4.88	4.27	3.86	5.24	3.82
Tb	0.50	0.55	0.61	1.05	0.87	0.53	0.81	0.63
Dy	3.05	3.59	3.77	7.13	5.55	2.69	4.58	3.63
Ho	0.60	0.78	0.77	1.53	1.16	0.46	0.89	0.71
Er	1.87	2.67	2.39	5.28	3.84	1.36	2.54	2.08
Tm	0.28	0.41	0.36	0.83	0.59	0.17	0.39	0.31
Yb	1.98	2.88	2.27	5.65	3.99	1.17	2.36	1.94
Lu	0.31	0.44	0.36	0.84	0.60	0.17	0.31	0.29
Hf	0.71	1.36	3.00	3.23	2.91	8.93	9.12	5.83
Pb	14.93	<5	<5	<5	<5	15.57	6.59	8.70
Th	0.65	0.07	2.44	0.34	1.16	8.09	9.05	6.92
U	0.36	<0.05	1.78	0.17	0.39	1.43	1.00	0.86

The denotation m1–m3 relates to outcrops of mafic- to ultramafic rocks in the Pare mountains (Fig. 1). The abbreviations *am* (amphibolite) and *gn* (gneiss) refer to different tectonic units (roman numerals I, II, III, IV) in SE Kenya (Fig. 1). “Less than” symbol: not detected at this lower limit. Oxides and trace elements indicated in wt% and ppm, respectively. A minus (–) in the LOI line shows a gain on ignition. *amr* Amphibolitic rock. The rocks of site m1–m3 may be referred to as metapyroxene-hornblende-gabbro (147-1); hornblende bearing metagabbro (147-2); plagioclase bearing metahornblende-pyroxenite (147-3); metapyroxene-hornblende-gabbro (147-4); metahornblende-gabbro (147-5); spinel bearing hornblende-metagabbro (149-1); amphibolitic rock/mafic granulite (149-2, 152-0); hornblende-metagabbro (149-3, 149-4); spinel bearing metaclinopyroxenite (152-1); metagabbro (152-2)



are distinguished, denoted as Galana East (unit I)- and West (unit II, or synonymously, Galana River shear zone), Transition zone (unit III) and Taita Hills (unit IV) (Fig. 1). This subdivision (see also Hauzenberger et al. 2004) corresponds to the Sobo formation in the eastern Galana River profile (unit I) and the contiguous Lugard's Falls belt (unit II). Unit IV, the Taita Hills, cover portions of the Kurase Kasigau group (Horkel et al. 1979). A narrow domain containing ridge-shaped gneisses (unit III) extends from the Sagala Hills towards NNW (Fig. 1) and marks the change between the Taita Hills (unit IV) and the Galana River shear zone (unit II).

New age data (U–Pb zircon) from SE Kenya indicate several metamorphic and magmatic events (Hauzenberger et al. 2007). Granulite facies conditions (Hauzenberger et al. 2004) ranging from  $644 \pm 15$  to  $629 \pm 6.8$  Ma can be found in unit II, unit III and unit IV. A granulite facies event at about  $550 \pm 14$  Ma is indicated for unit I. Igneous ages derived from metagranitoid samples indicate  $970 \pm 14$  Ma (unit II) and  $955 \pm 44$  to  $845 \pm 20$  Ma (units III–IV), a younger emplacement age ( $644 \pm 15$  Ma) was detected in unit IV. Deformed pegmatitic rocks (sampled from unit II) yield crystallization ages of  $580 \pm 9.7$  and  $564 \pm 7.4$  Ma. Pre-Pan-African basement is indicated by zircon xenocrysts (unit IV and unit II;  $\sim 1.4$ – $1.0$  Ga).

### NE Tanzania

The NW–SE trending range of the Pare–Usambara mountains in NE Tanzania (Fig. 1; Bagnall 1960; Bagnall et al. 1963; Dundas 1965; Hartley and Moore 1965) consists of granulitic gneisses which are mainly enderbitic in composition (e.g., Appel et al. 1998). Intercalated rocks comprise metasediments, marbles, calc-silicates, and mafic to ultramafic rocks. In the North-Pare mountains (Fig. 1) horn-blende-, pyroxene-, quartz-feldspar- and calc-silicate granulites are frequent. Enclosed are kyanite-, graphite- and biotite gneisses and schists, quartzites, marbles and amphibolites. They often occur as variably sized layers or lenses. Mafic to ultramafic rocks consist of metagabbroids, metapyroxenites and serpentinites. Meta-anorthosites are exposed, e.g., at Ikongwe (Dundas 1965, Fig. 1) and near Mahunga peak (Bagnall 1960; Fig. 1). The Ikongwe anorthosite has a marginal planar structure which passes into a more massive character with corona textures (garnet around hornblende and pyroxene), whereas the small analogue (about two km NE of Mahunga peak) is banded. Banded garnet-, pyroxene- and hornblende granulites are common in the South-Pare mountains. Graphite gneisses occur as thin layers. The ultramafic rocks include serpentine, olivine, spinel, amphibole, clinopyroxene, orthopyroxene, plagioclase, garnet, scapolite, epidote, titanite and chromite (Dundas 1965).

In addition to the above-mentioned lithologies, distinct bands of hornblende-pyroxene granulites are present in the Usambara mountains. Biotite gneisses are usually better exposed in the western peneplain of the Usambara- and also Pare mountains. Calc-silicate rocks, marbles, quartz-feldspar gneisses and metapelites are dominant in the Uмба Steppe which form the NE lowlands (Hartley and Moore 1965; Fig. 1). Typical Pare–Usambara granulites are rare in the NE lowlands. Mafic to ultramafic rocks occur, beneath a large serpentinite near Uмба (Fig. 1, Hartley and Moore 1965; Solesbury 1967).

Structurally, the Pare–Usambara mountains preserve a gently ( $\sim 20^\circ$ ) E–ENE dipping foliation whereas lineations are widely scattered. Rocks of the Uмба Steppe occasionally record steeper easterly dipping foliations ( $55^\circ$ – $80^\circ$ ). Recumbent folds are widespread with axes mostly trending to the NE (Bagnall 1960; Bagnall et al. 1963; Dundas 1965). NW trending fold axes document cross folding in the North Pare mountains. Minor warping (NNW trending axes) can be found in the Usambara mountains. Recumbent isoclinal folds and two periods of folding were also reported from the Uмба Steppe area (Hartley and Moore 1965). Shackleton (1993) indicated a strain gradient for different structural levels in the Usambara mountains. In addition he noticed thrust tectonics (SW–WSW vergence) and the occurrence of sheath folds.

Recent petrological studies (e.g., Appel et al. 1998) show high pressure granulite facies conditions for the area. Peak metamorphism in the Pare mountains occurred at 645–640 Ma (Muhongo and Lenoir 1994; Möller et al. 2000) while the Usambara mountains show  $\sim 625$ – $641$  Ma (Möller et al. 2000; Muhongo et al. 2001). Rocks from the Uмба Steppe experienced high grade metamorphism at about 617–620 Ma (Möller et al. 2000).

### Sampling and analytical methods

A total of 36 specimen of metabasic rocks and orthogneisses were analyzed (Table 1). The data from the literature consist of mafic- to ultramafic rocks (Frisch and Pohl 1986; 20 samples) and orthogneisses and metagranitoids (7 samples, Maboko and Nakamura 2002; 13 samples, Kröner et al. 2003). In SE Kenya, amphibolites occur as thin layers and small lenses usually aligned with the regional trend of host rocks often formed by migmatitic gneisses. From the Galana River area (units I–II; Fig. 1) five gneisses and eight amphibolites were investigated, among them three metabasites from a site west of Lugard's Falls (Fig. 1). Five gneisses are from the Transition zone (unit III), three amphibolites and three gneisses were sampled from the Taita Hills (unit IV). The amphibolites are from both the Kurase- and the Kasigau group (Fig. 1).

Mafic to ultramafic rocks from NE Tanzania were sampled from three sites (Fig. 1), located at the northern foothills of the Pare Mountains at m3 (Fig. 1) or SE to ESE of Same (Fig. 1) at m1 and m2. The exposures appear as isolated lenses and include several rock types at each outcrop. Twelve samples were analyzed, five from site m1, four from site m2 and three from site m3.

Major and trace element analyses of metabasic and gneissic samples (this study; Table 1) were performed at Activation Laboratories Ltd in Ancaster (Ontario), Canada, using ICP-AES and ICP-MS techniques. Calibrations were made using reference samples and international standards. Relative standard deviations are <1% for SiO<sub>2</sub> and <2% for the other major elements, except MnO and P<sub>2</sub>O<sub>5</sub> ( $\pm 0.01\%$ ) and K<sub>2</sub>O ( $\pm 0.005\%$ ). Relative standard deviations for trace elements are generally <5%. Lower limits of detection were reached for P<sub>2</sub>O<sub>5</sub> (0.01 wt%), Be (1 ppm), Cr (20 ppm), Ni (20 ppm), Cu (10 ppm), Zn (30 ppm), Li (0.5 ppm), Rb (2 ppm), Cs (0.1 ppm), Hf (0.1 ppm), Pb (5 ppm), and U (0.05 ppm). The determination of structurally bound H<sub>2</sub>O was made via loss on ignition (LOI).

## Petrography

### Metabasic (ultrabasic) rocks

In addition to amphibole-plagioclase-quartz, the amphibolitic rocks from SE Kenya contain  $\pm$ garnet,  $\pm$ biotite,  $\pm$ clinopyroxene,  $\pm$ orthopyroxene,  $\pm$ scapolite,  $\pm$ ilmenite,  $\pm$ titanite (Hauzenberger et al. 2004). Amphibole occurs as 0.3–5 mm grains, garnet (1–3 mm) often show inclusions (quartz, plagioclase, ilmenite) and coarse grained foliated fabrics dominate.

The mafic to ultramafic samples of the Pare mountains (NE Tanzania, m1–m3) indicate metagabbroic to garnet-bearing amphibolitic/mafic granulite rocks (rock names are given in the caption of Table 1). The investigated rocks show a variable amount of amphibole, clinopyroxene, plagioclase,  $\pm$ orthopyroxene,  $\pm$ garnet,  $\pm$ spinel,  $\pm$ scapolite,  $\pm$ magnetite,  $\pm$ hematite,  $\pm$ zoisite. Accessory minerals are, e.g., apatite, ilmenite and  $\pm$ quartz. The fabrics are usually coarse grained and often display granoblastic texture. The grain size (amphibole, pyroxene, plagioclase) varies from 0.5 to 5 mm (average size  $\sim 0.1$ –2 mm). Frequently, an intergrowth of spinel and an opaque phase appears, symplectitic intergrowth (garnet-opaque phase) is also present. Poikiloblastic garnets contain, e.g., pyroxene, amphibole, plagioclase or opaque inclusions. In addition metamorphic rims can be found, with either garnet around clinopyroxene or clinopyroxene around orthopyroxene.

### Gneisses (metagranitoids)

The main mineral assemblages of the investigated gneisses (SE Kenya profile; Fig. 1) include amphibole–plagioclase–quartz–biotite,  $\pm$ K-feldspar,  $\pm$ garnet,  $\pm$ Fe-oxide (Hauzenberger et al. 2004). Clinopyroxene, ilmenite, and  $\pm$ titanite occur additionally in the rocks of unit III and the Taita Hills (unit IV). Amphibole ranges in size from 0.1 to 5 mm. Biotite, usually present as flakes, often shows dimensions of 0.1–2 mm. When garnet is present, it forms mostly inclusion free grains of 0.1–3 mm size. In general, the fabrics of the investigated rocks indicate a well foliated gneissic texture.

### Analytical results (geochemical classification)

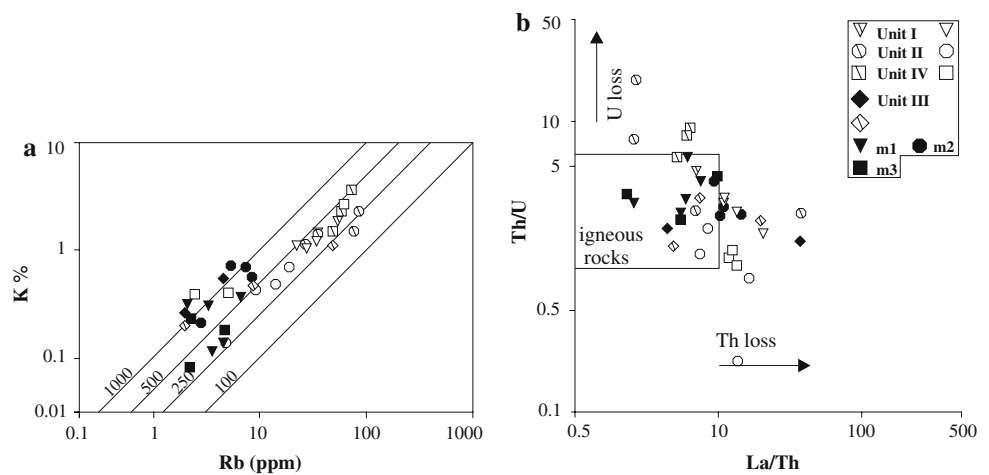
**Element mobility** High-field strength elements (HFSE) and REE are least mobile during metamorphic processes (e.g., amphibolite facies, Polat et al. 2003). Consequently, HFSE and REE are most likely to preserve the original protolith signatures of the samples in this study. Chondrite normalized REE plots show consistent patterns (Figs. 5, 7) and define a coherent data set. Consequently we focus on these elements in the following discussion.

To test the mobility of LILE, we use, e.g., element ratios including K/Rb, Th/U and La/Th (Fig. 2a, b; see Rudnick et al. 1985; Stephenson 2000). About two third of the data (Fig. 2a) plot within the array of K/Rb ratios that has been observed in igneous rocks (e.g., Shaw 1968; Rudnick et al. 1985). Higher values (e.g., K/Rb > 550; Table 2) are to be found in some basic- to ultrabasic rocks (m1–m3), amphibolite (unit IV) and gneiss samples (unit IV), but are consistent with values reported, e.g., from oceanic settings (e.g., Gill 1981; Sun and McDonough 1989; Coleman 1977). A La/Th–Th/U plot (Fig. 2b) suggests that some gneiss- and amphibolite samples are depleted in U and Th. Since, however, MORBs have higher La/Th values (La/Th > 10; Table 2), the values of the amphibolitic rocks could be correct. For two gneiss samples from unit III (K209, K154; Table 1), the U and Th depletion (and high La/Th ratios) might be explained by retention of U and Th in accessory phases (e.g., zircon, see discussion and references in Rudnick et al. 1985). Both samples exhibit low U and Th concentrations (<0.4 ppm), and for zircons of sample K209 (filled diamond; Fig. 2b) a low Th/U ratio (Th/U  $\sim 1.5$ ) was also noted (Hauzenberger et al. 2007). In conclusion, we note some mobility in LILE and therefore prefer to restrict the following discussion to the REE and HFSE.

### Amphibolitic rocks

A magmatic origin of amphibolitic rocks from SE Kenya is indicated by a Niggli c-mg plot (Leake 1964; Fig. 3a). Two

**Fig. 2** Plot of **a** K/Rb ratios (e.g., Shaw 1968) and **b** Th/U versus La/Th (both plots after Rudnick et al. 1985). The rectangle in **b** represents the common field of igneous rocks (other than MORB, see text). Gneisses are marked by hatched symbols (except two samples (filled diamonds; unit III); see Fig. 7)



samples from the Galana River shear zone (unit II) deviate from the magmatic trend, but high Cr values ( $>450$  ppm, Table 1) suggest an igneous protolith. This is supported by a trace element discrimination (Winchester et al. 1980) (see below Fig. 6b) in which all amphibolites plot within the magmatic field. Thus we infer a magmatic protolith for the amphibolitic rocks. In the TAS diagram (Le Bas et al. 1986) the amphibolitic precursors are suggested to be basalts, basaltic andesites or basaltic trachy-andesites. However, using less mobile trace elements (e.g., Winchester and Floyd 1977; Fig. 3b) the rocks mostly range from sub-alkaline basalt to andesite/basalt. Only the Kurase group amphibolites are alkaline. Moreover, most of the samples suggest a tholeiitic source which follows from trace elements (Fig. 3c; Piercey et al. 2004; Lentz 1998).

Selected trace element variation plots (Fig. 4a–d) suggest varying degrees of element enrichment between samples of the Galana River region (eastern unit I and western unit II). Furthermore, differences are seen also in chondrite-normalized REE patterns (Fig. 5a). Amphibolites of unit I show absolute LREE enrichment ( $La \approx 45\text{--}65\times$  chondrite;  $La_n/Lu_n \approx 2\text{--}7$ ) and relative overall multiple element enrichments compared to the rocks of unit II ( $La \approx 11\text{--}16\times$  chondrite;  $La_n/Lu_n \approx 1.4\text{--}2.5$ ). The latter are characterized by flatter LREE and relatively depleted HREE. As in Fig. 4a–d, a sample of unit I ( $La \approx 43\times$  chondrite;  $La_n/Lu_n \approx 7$ ) shows an intermediate position regarding the concentration of REE. The Taita Hills amphibolites (unit IV) (Fig. 5b) show two trends: LREE enrichment ( $La \approx 8.5\text{--}23\times$  chondrite;  $La_n/Lu_n \approx 7\text{--}7.5$ ) and slightly positive Eu anomalies that are typical for the specimens of the upper Kurase group. The Kasigau sample exhibits a more uniform pattern ( $La \approx 17\times$  chondrite;  $La_n/Lu_n \approx 1.2$ ).

#### Metabasic- and ultrabasic rocks (site m1–m3)

Chondrite-normalized REE plots indicate different concentration patterns for the mafic and ultramafic rocks (site

m1–m3). Two REE patterns are present in a lense SE of Same (m1; Figs. 1, 5c). Three samples are enriched in all REE ( $La \approx 8\times$  and  $66\text{--}100\times$  chondrite;  $La_n/Lu_n \approx 2.6$  and  $4.3\text{--}4.5$ ) and show the ratios decline until Ho and slightly rise towards Lu. Two samples show minor enrichment relative to chondrite of LREE ( $La_n \approx 3\text{--}3.2\times$  chondrite;  $Sm_n \approx 0.5\text{--}0.8$ ) with a distinct Eu peak and increases in values up to Lu. Mixed sources are quite likely documented in the lense ESE of Same (m2; Figs. 1, 5d). While two samples are slightly depleted in LREE ( $La_n/Lu_n \approx 0.4\text{--}0.5$ ;  $La_n \approx 7.1\text{--}7.3\times$  chondrite) the other samples show considerable LREE concentrations relative to chondrite ( $La_n \approx 65\text{--}165\times$  chondrite) and low to moderate enrichment relative to the HREE ( $La_n/Lu_n \approx 2.4\text{--}13$ ). More uniformly enriched patterns were derived from the northernmost occurrence m3 (Fig. 1). Gabbroic specimens (Fig. 5e) plot near the chondritic reference line ( $La \approx 1.7\text{--}2\times$  chondrite;  $La_n/Lu_n \approx 0.9\text{--}1.5$ ) and show small LREE troughs with positive Eu anomalies. A garnet-bearing sample of the same location shows a uniform enrichment of all REE ( $La \approx 16\times$  chondrite;  $La_n/Lu_n \approx 1$ ).

#### Gneisses (metagranitoids)

Indications about the origin of gneisses can be gained using, e.g., a  $SiO_2\text{--}TiO_2$  plot (Tarney 1977) (Fig. 6a). The geochemistry of the gneisses plot in the field of igneous rocks or close to the border separating sedimentary and igneous protoliths. The sample of unit I shows a higher  $TiO_2$  value which may indicate a sedimentary precursor. A similar division can be made purely on trace elements (Winchester et al. 1980; Fig. 6b). Many gneisses show Ni values lower than the detection limit (Table 1). Thus if we also consider a shift towards the ordinate of the graph most of the samples indicate an igneous source. This agrees with A/CNK ratios (Chappell and White 1974; Table 1) suggesting

**Table 2** Comparison of the data (using different element ratios) with data from present-day tectonic settings

	N-MORB		E-MORB	OIB	Volc.Arc	Back Arc	Unit I			Unit II			Unit IV			
	A14	F2					KTB98	K57	KGB27	K108	KGB173	K108	KGB49A	AKTB55	KTBI75	KTBI75
Ba/La	2.5 <sup>S</sup> 4-11 <sup>G</sup>	9 <sup>S</sup> 11-20 <sup>G</sup>	9.5 <sup>S</sup>	12-100 <sup>G</sup>	4-21 <sup>G</sup>	71	46	15	16	61	25	38	27	30	11	31
Ba/Nb	2.7 <sup>S</sup>	6.9 <sup>S</sup>	7.3 <sup>S</sup>	35-96 <sup>P</sup>	8-34 <sup>P</sup>	192	278	27	26	562	113	128	112	61	11	24
La/Nb	1-2 <sup>S</sup>	<1 <sup>S</sup>	<1 <sup>S</sup>	2-5 <sup>G</sup>	1-2(7) <sup>G</sup>	2.7	6	1.7	1.6	9.3	4.5	3.3	4.1	2.1	1	<1
La/Th	20.8 <sup>S</sup> 15-25 <sup>G</sup>	10.5 <sup>S</sup> 7-15 <sup>G</sup>	9.3 <sup>S</sup>	2-10 <sup>G</sup>	<1-3 <sup>P</sup>	20	11	13	11	7	16	8.5	14	12	13	14
Ba/Rb	11.3 <sup>S</sup>	11.3 <sup>S</sup>	11.3 <sup>S</sup>	9-48 <sup>T</sup>	9.5-28 <sup>P</sup>	28	27.6	9.7	9.5	33.4	20.3	9.5	6.7	30.3	37.1	11.2
K/Rb	1071 <sup>S</sup>	417 <sup>S</sup>	387 <sup>S</sup>	339-760 <sup>P</sup>	160-635 <sup>P</sup>	406	492	374	346	470	290	347	367	786	1587	419
	ml															
	m2															
	m3															
	147-1	147-2	147-3	147-4	147-5	149-1	149-2	149-3	149-4	152-0	152-1	152-2				
La/Th	5.5	2.6	6.1	7.5	5.9	14.5	10.3	9.3	10.9	9.9	5.4	2.3				
K/Rb	1504	541	306	319	925	766	938	1337	662	1019	375	387				
Ba/Rb	20.5	5.4	144.1	15.5	361.4	69.6	52.6	45.2	83.3	31.9	8.2	31.1				
K <sub>2</sub> O/Na <sub>2</sub> O																
	Unit I						Unit II			Unit III			Unit IV			
	K13	Mb153	KGB35LF	KGB170	KGB49C	K115	K209	KGB174	K154	K120	K37	KTBI46A	MDB			
4.2-24.4 <sup>H</sup>	7.0	37.5	2.6	2.7	7.0	4.4	37.3	4.8	19.6	7.4	5.2	6.4	6.0			
394(732)-581(7581) <sup>H C</sup>	333	428	263	394	191	1192	1328	226	996	536	389	474	295			
7.5-308.5 <sup>H</sup>	9.3	31.3	16.6	14.3	8.3	48.0	34.5	8.6	55.6	31.7	14.3	12.5	12.3			
<0.1-0.3(0.4) <sup>C H K</sup>	0.6	0.3	0.7	0.4	0.5	0.2	0.1	0.4	0.1	0.2	0.6	1.1	0.4			

Superscripts: S (Sun and McDonough 1989); G (Gill 1981); P (Pearce 1982); D (D'Orazio et al. 2004); T (Taylor and Nesbitt 1998). Upper table: amphibolitic rocks (SE Kenya). Lower table: ultrabasic- to basic rocks (NE Tanzania) and gneisses (SE Kenya). K<sub>2</sub>O/Na<sub>2</sub>O ratios are only listed for gneisses. Range of data (gneisses): H (Haraguchi et al. 2003)—Komahashi-Daini Seamont tonalite suite; C (Coleman 1977)—plagiogranites (Troodos ophiolite; values in brackets); K (Koepeke et al. 2004)—ophiolitic plagiogranites from different supra-subduction-zone settings (data compiled from literature)

**Fig. 3** Mafic-Ultramafic rocks and amphibolites. **a** Plot using Niggli c and mg (after Leake 1964). **b** Trace element discrimination after Winchester and Floyd (1977). **c** Tholeiitic/calk-alkaline classification from Piercey et al. 2004 (after Lentz 1998)

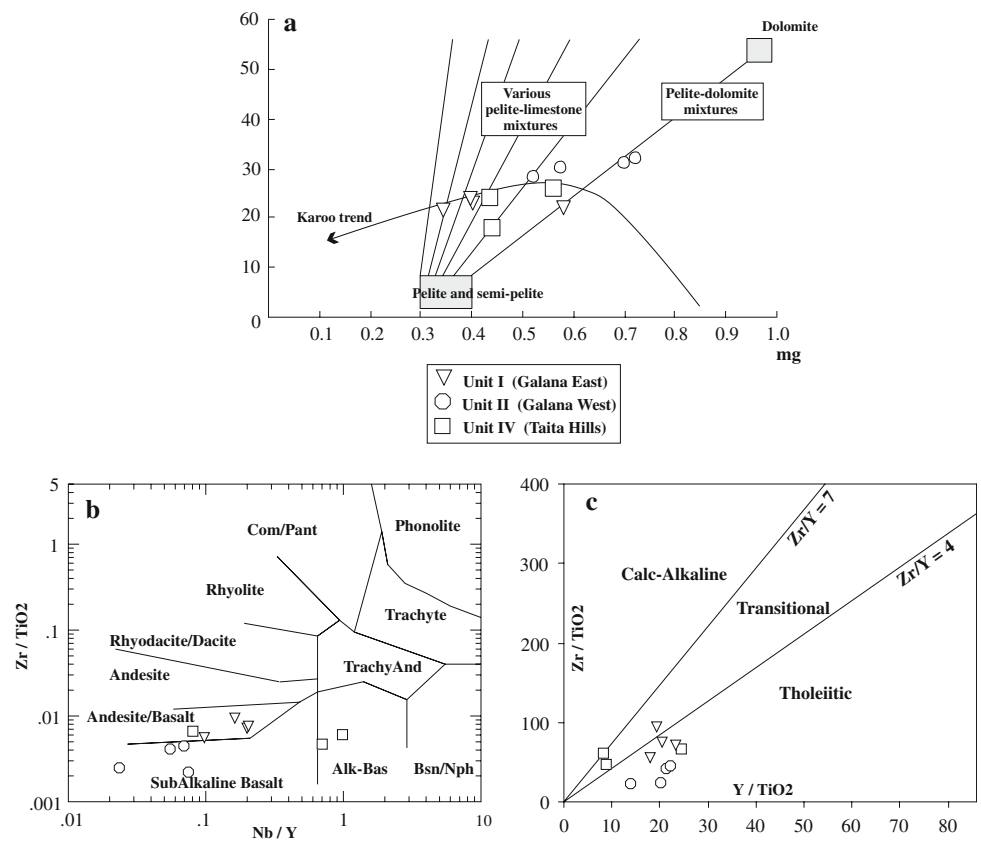


**Fig. 4 a–d** Selected trace element variation diagrams for amphibolitic rocks from SE Kenya (units I, II, IV)

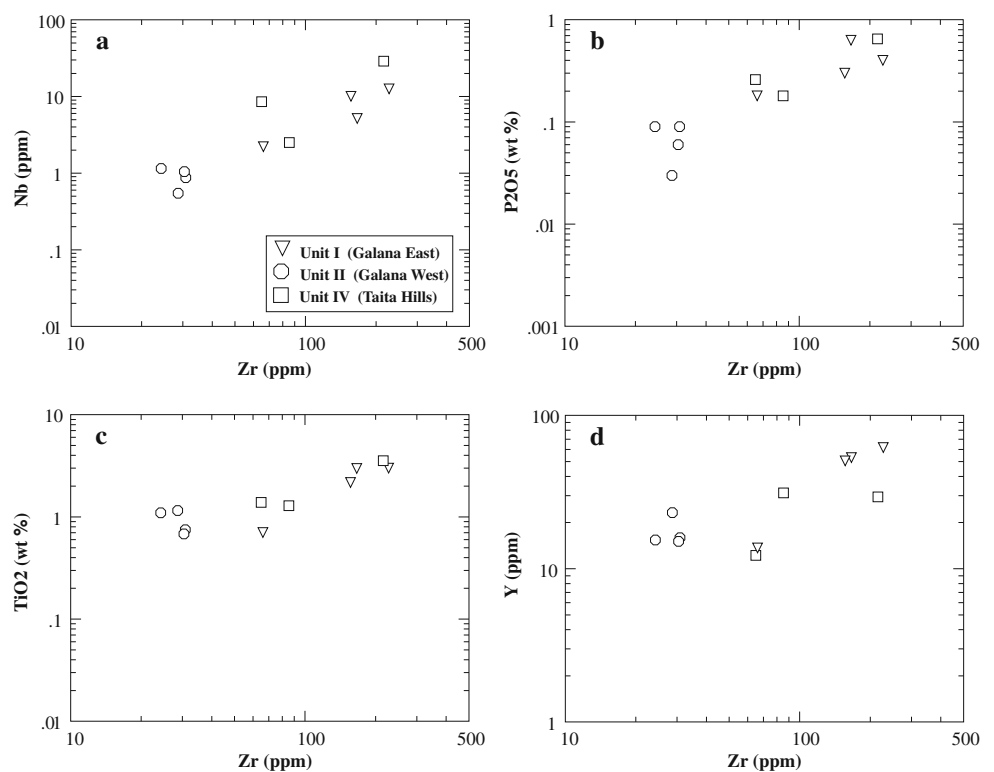
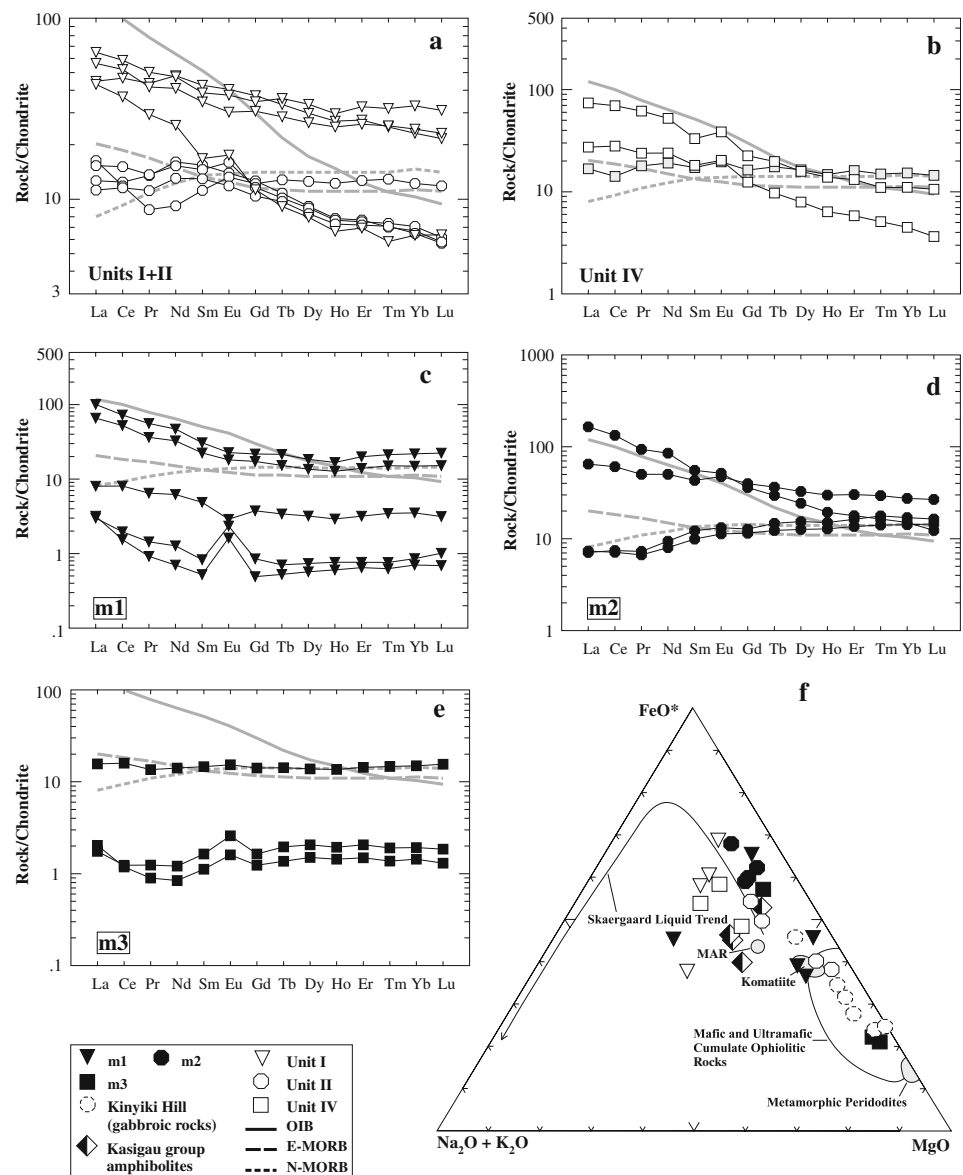


**Fig. 5** REE distributions of amphibolites **a** for units I–II and **b** unit IV (for clarity the sample from the Kasigau group **b**) is shaded). **c–e** REE patterns of ultramafic- to mafic rocks (NE Tanzania; m1–m3). Chondrite values from Boynton (1984), average N-MORB, E-MORB and OIB (oceanic island basalt) composition from Sun and McDonough (1989). **f** AFM diagram (after Coleman 1977), see discussion below. *Filled triangles* m1; *filled circles* m2; *filled squares* m3. *Open circles (dashed)* gabbroic cumulates from Kinyiki Hill (Frisch and Pohl 1986)



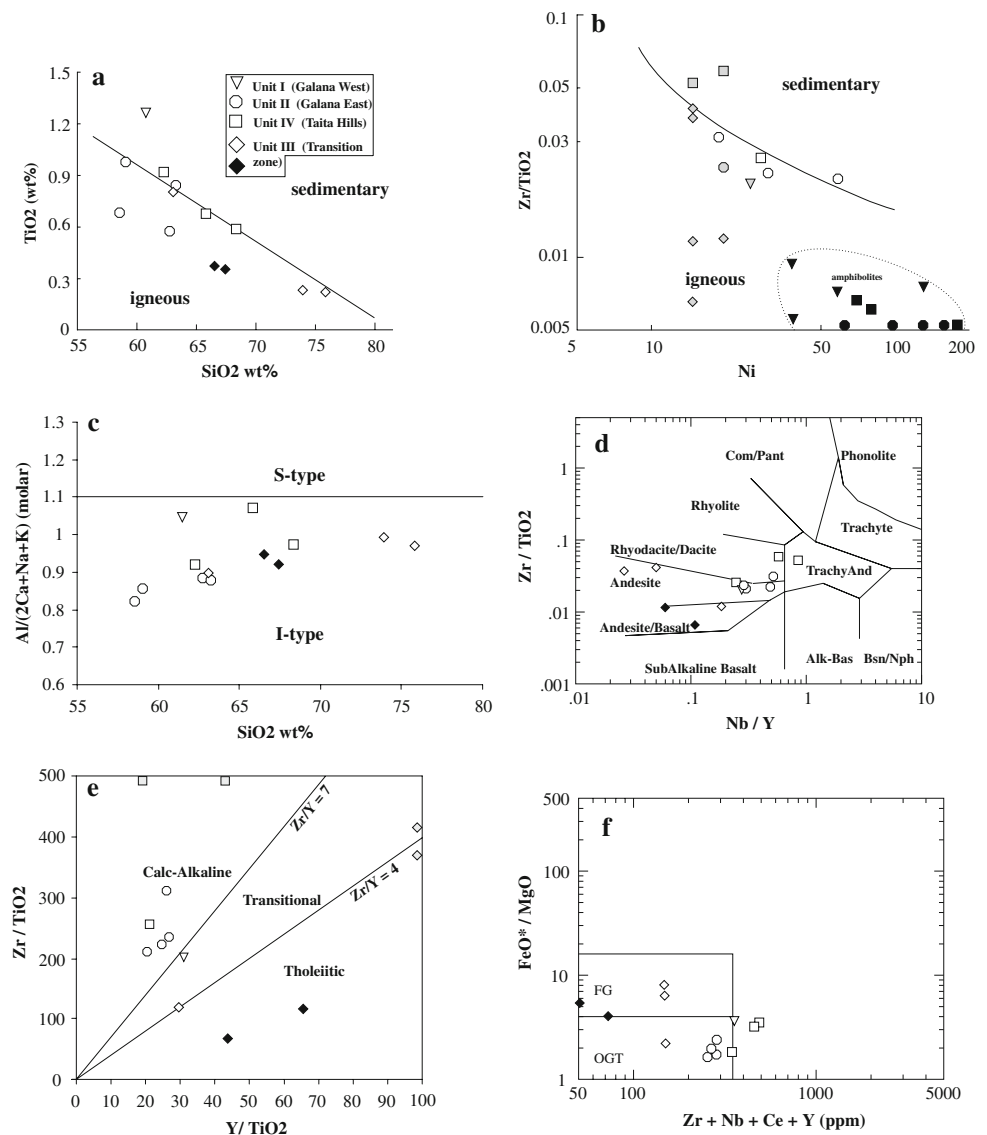
I-type granitic origin (Fig. 6c) for the meta- to weakly peraluminous rocks (Shand 1927). According to the discrimination of Debon and Le Fort (1983) (plot not shown) the rocks are tonalitic to granodioritic in composition, with subordinate quartz diorite and adamellite. Likewise, the trace element subdivision (Winchester and Floyd 1977; Fig. 6d) mostly show basaltic-andesite to dacite composition. Other than gneisses of unit III which indicate tholeiitic differentiates, the rocks suggest a calc-alkaline source (Fig. 6e).

These variations are displayed by the REE plots (Fig. 7). Similar REE enrichment patterns exist for the Taita Hills (IV) ( $La_n/Lu_n \approx 15\text{--}25$ )—and Galana River shear zone (II) gneisses ( $La_n/Lu_n \approx 87\text{--}127$  chondrite;  $La_n/Lu_n \approx 10\text{--}21$ ), a higher REE content (M- to

HREE) appears for the sample of unit I ( $La \approx 91 \times$  chondrite;  $La_n/Lu_n \approx 5$ ) (Fig. 7a, b). Gneisses of unit III (Fig. 7c) differ in REE concentrations (e.g., LREE- and HREE) and indicate two groups. Contrary to rocks of the other units they also show negative or positive Eu anomalies. The first group (filled diamonds; Fig. 7c) is more consistently enriched in REE ( $La \approx 2.8\text{--}2.9 \times$  chondrite;  $La_n/Lu_n \approx 0.7\text{--}1.0$ ), one sample exhibits a positive Eu anomaly. In addition to negative Eu anomalies in the other group ( $La \approx 21\text{--}28 \times$  chondrite;  $La_n/Lu_n \approx 0.8\text{--}1.5$ ), one sample resembles gneisses of the neighbouring unit without an anomaly (Fig. 7c). LREE of the sample are most enriched ( $La \approx 39 \times$  chondrite;  $La_n/Lu_n \approx 3.4$ ) and the MREE to HREE follow the patterns of gneisses of unit II and unit IV.



**Fig. 6** Discrimination between sedimentary and igneous origin of gneisses. **a** Plot after Tarney (1977), **b** Winchester et al. (1980) and **c** Chappell and White (1974). **d** Trace element classification (Winchester and Floyd 1977). **e** Y/TiO<sub>2</sub> versus Zr/TiO<sub>2</sub> plot from Pearcey et al. 2004 (after Lentz 1998). **f** Characterization after Whalen et al. (1987). OGT unfractionated M-, I- and S-type granites. FG fractionated felsic granites. Amphibolite data <0.005 ppm adjoin to the x-axis. Shaded symbols **b** Ni values below detection limit; **e** values greater than scale



## Geotectonic interpretation

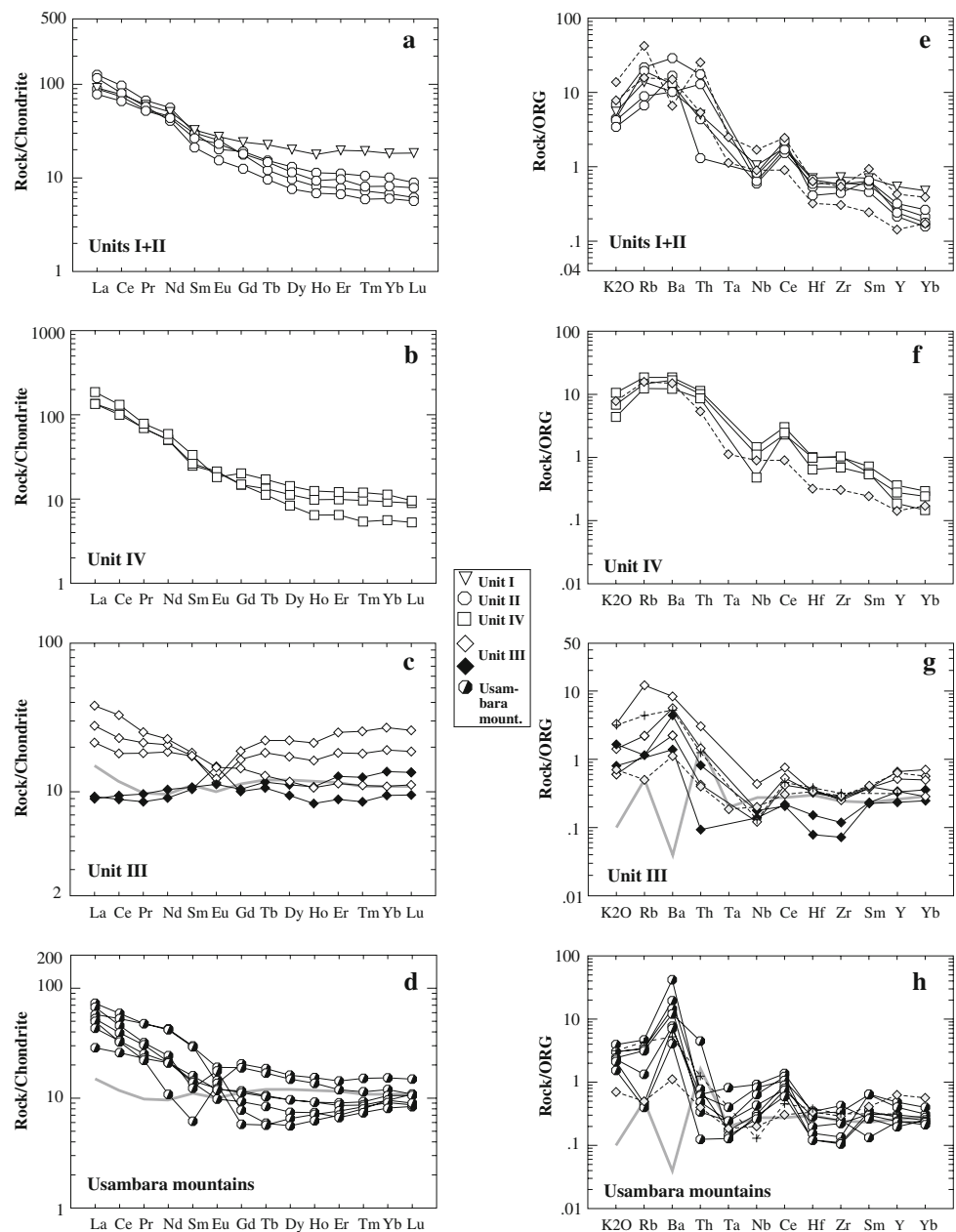
### Amphibolitic rocks

MORB-normalized plots (Pearce 1982) are used to suggest possible tectonic settings. The samples from the Galana River shear zone (unit II) (Fig. 8a) display a significant depletion of HFS (Nb, Hf, Zr) and considerable enrichment of LIL elements (Sr to Th). Different patterns are shown by the rocks of unit I (Fig. 8b), which show greater LIL enrichments. The other samples define peaks in Ba and, in one case, show a sudden decline from Th to Nb. Several patterns are also displayed for the Taita Hills samples (unit IV; Fig. 8c, d). The amphibolite from the Kasigau group (Fig. 8c) indicates a characteristic MORB signature from Ce to Sc, apart from more enriched P<sub>2</sub>O<sub>5</sub>. The only LIL with higher concentration is Ba, a smaller Nb anomaly can

also be seen. The Kurase group patterns (Fig. 8d) differ in part by a greater element abundance (Sr to P<sub>2</sub>O<sub>5</sub> or TiO<sub>2</sub>) and are depleted from Y to Sc. A marked difference is the lack of a Nb anomaly.

Thus based on geochemistry, one can conclude that several sources or tectonic settings might be involved in the formation of the amphibolites. The distinct Nb, Hf and Zr element depletion coupled with enrichment of LIL for rocks of the Galana River shear zone (unit II) and two samples of unit I (Fig. 8a, b) suggest the influence of a subduction process. The rocks from the upper Kurase group (Fig. 8d) do not show these characteristics and also differ from MORBs in their more varying element concentrations (Nb to Cr). Within-plate sources can be distinguished, e.g., by means of Nb/Y versus Ti/Y ratios (Pearce 1982; Fig. 8e). The plot suggest a transitional setting for the samples (Nb/Y ≈ 0.7–1) as can be found, e.g., at continental rifts.

**Fig. 7** REE distributions for gneisses of **a** unit I–II, **b** unit IV, **c** unit III, and **d** Maboko and Nakamura (2002) (circles half-filled). Bold grey line in **c** and **d**, plagiogranite from the ophiolitic component of the Ankara mélangé (Dilek and Thy 2006). Norm values as in Fig. 5. **e–h** Ocean ridge granite (ORG)-normalized plots (and reference data) from Pearce et al. (1984). **e** Gneisses (unit I–II) and reference from Jamaica and Chile (dashed lines and shaded diamonds). **f** Gneisses (unit IV) and the Jamaica granite. **g** Gneisses (unit III) and reference from Oman (shaded diamonds), New Britain (crosses, Whalen et al. 1987) and the Ankara mélangé (bold grey line). **h** ORG-normalized plot (data from Maboko and Nakamura 2002), reference data as in **g**. For a discussion (e–h), see text



This is consistent with results of Frisch and Pohl (1986) (10 samples;  $Nb/Y \approx 0.2-0.5$ ) who proposed a rift related origin for the Kurase group (Fig. 8e). Considering a volcanic arc setting, rocks of the Kurase group as well may be associated with back-arc spreading. This option is tested using  $Zr/Ti$  against  $Zr$  behaviour (e.g., Woodhead et al. 1993; Fig. 8f). From this it follows that data from the Kurase group would be compatible with a back-arc origin. Thus some of the mafic to ultramafic lenses in the Taita Hills may relate to such a setting.

The samples from unit II ( $Nb/Y < 0.1$ ) have compositions consistent with island arc basalts (Figs. 8e, f; 9a, b).

The amphibolite from the Kasigau group ( $Nb/Y < 0.1$ ) and those from unit I ( $Nb/Y \approx 0.1-0.2$ ) fall mainly into the common field of volcanic arc to MORBs (Fig. 8e). This is also noted from tectonic discrimination plots after Wood (1980) (Fig. 9a) and the Basaltic Volcanism Study Project (1981) (Fig. 9b). The rocks from unit I those are less depleted or enriched in HFS elements (Fig. 8b) lie marginally or in between the discrimination fields (Fig. 9a). Again, the Kurase group samples plot in a separate position (within-plate basalts). In the  $La/Sm-Ba/La$  plot (Fig. 9b), samples of unit I plot in the overlapping field of MORB and island arcs.



**Fig. 8** MORB-normalized plots (after Pearce 1982) for amphibolites. **a–b** Unit I–II; **c** Kurase- and **d** Kasigau group (both unit IV). **e** Nb/Y–Ti/Y variations (Pearce 1982). Published data (Frisch and Pohl 1986), *dotted line* (array of Kurase group amphibolites), *diamonds half-filled* (Kasigau group amphibolites from Kinyiki Hill; Fig. 1). **f** Ti/Zr–Zr plot (after Woodhead et al. 1993). *Continuous lines* array of island arc basalts (IAB) and back-arc basin basalts (BAB) from Knittel and Oles 1995 (after Woodhead et al. 1993). *Dotted* (IAB; Kermadec arc-) and *dashed lines* (BAB; offshore Taupo volcanic zone) from Gamble et al. 1993, 1995) as well as MORB field (Klein et al. 1991). Published data: Kurase group amphibolites now shown as open diamonds. In addition, two amphibolites from the Kasigau group (Manyani Quarry; Fig. 1) are shown (Zr < 50 ppm; not pictured in Fig. 5e). *Shaded symbols* (e–f) values greater than scale. VAB volcanic arc basalt, WIP within-plate basalt

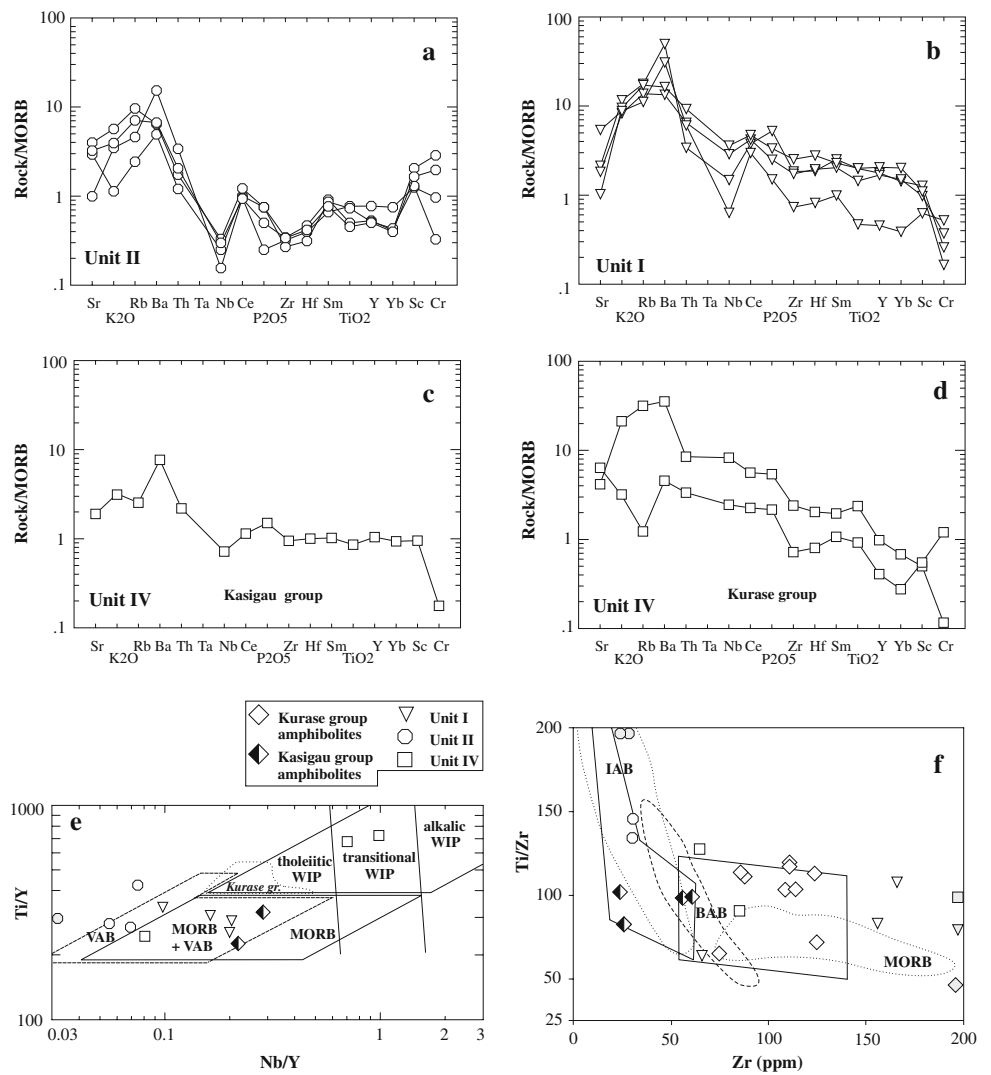
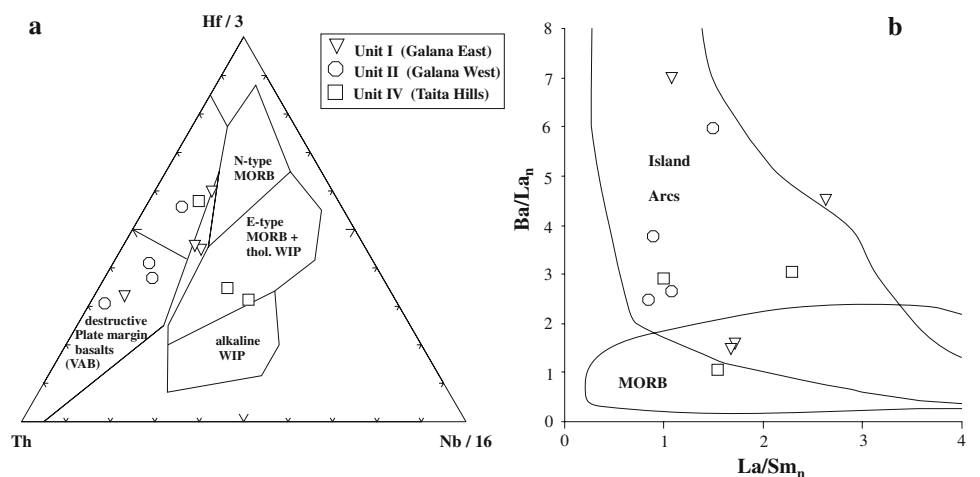


**Fig. 9** Tectonic discrimination plots after **a** Wood (1980) and **b** Basaltic Volcanism Study Project. Norm values in **a** as in Fig. 5

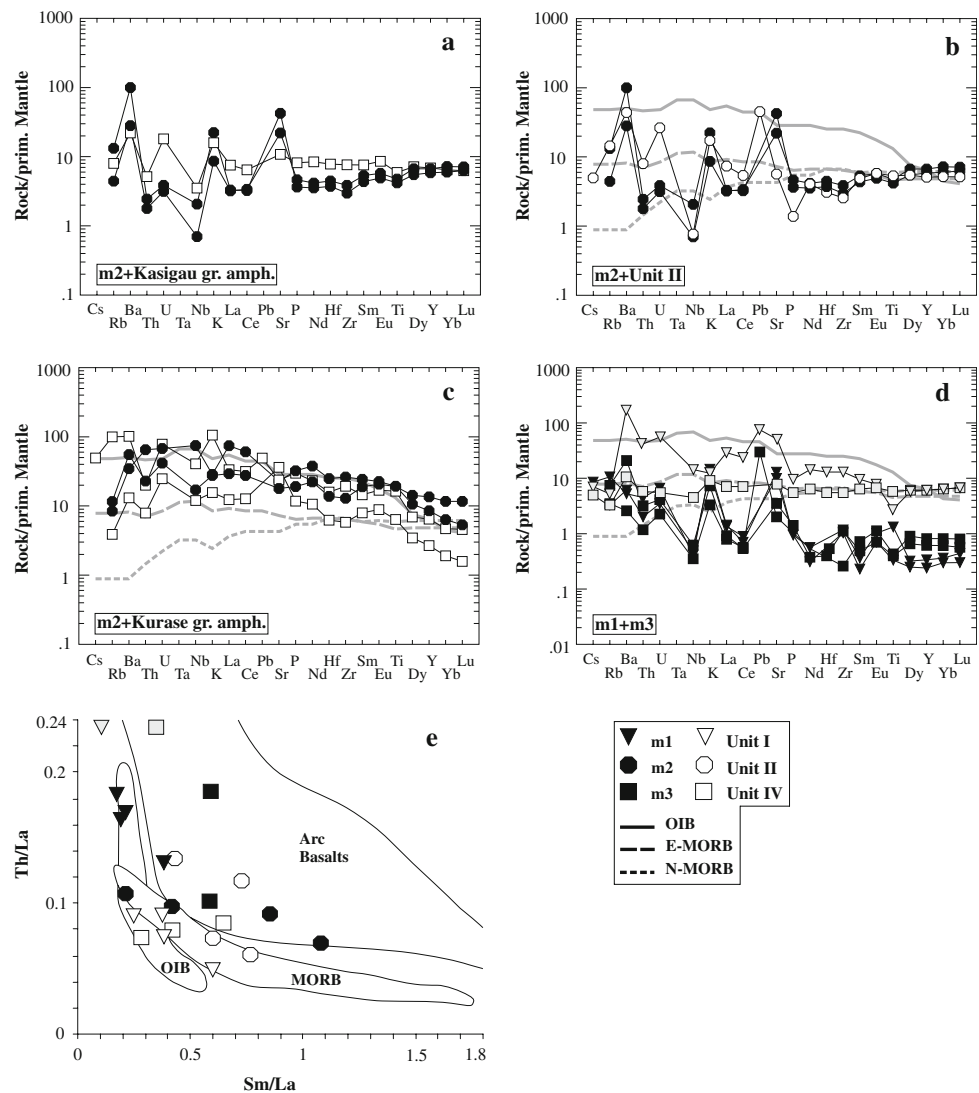


Metabasic- and ultrabasic rocks (site m1–m3)

For further classification the data are plotted in an AFM diagram (Fig. 5f; Coleman 1977). In addition, amphibolitic

rocks (units I, II, IV) and some data of Frisch and Pohl (1986) are pictured. In order to compare the data of different regions of the study area, we use multi-element diagrams (normalized to primitive mantle, Fig. 10a–d).

**Fig. 10** Mantle-normalized plots (norm values and average basalt compositions from Sun and McDonough 1989). The rocks showing LREE depletion (site m2) are compared **a** with the Kasigau amphibolite (Fig. 5b) and **b** a sample from unit II (Fig. 5a). **c** The rocks showing LREE enrichment (site m2) are displayed with the Kurase group amphibolites (Fig. 5b). **d** Comparison of the rocks from m3 with samples from m1 (for clarity two samples are shaded, respectively, including a sample from m1 with  $La \approx 66$  chondrite, Fig. 5c). **e** Sm/La versus Th/La plot including arrays of arc basalts, OIB and MORBs (after Plank 2005). Shaded symbols in **e** values greater than scale



The rocks are also evaluated on the basis of Th/La and Sm/La systematics (Fig. 10e) using Th/La ratios (deduced from subducting sediments) as an indicator for subduction processes (Plank 2005).

Four samples from the Pare mountains might be related to ophiolitic remnants including rocks from outcrops m3 and m1 (Fig. 5f). Two samples from site m3 plot into the field covering ophiolite type rocks and have typical  $Mg/(Mg + Fe_{tot})$  ratios of  $\sim 0.86$ . Rocks of m1 as well as two amphibolites of SE Kenya (both groups with  $Mg/(Mg + Fe_{tot}) = 0.70\text{--}0.73$ ) are situated at (near) the border which overlaps the array of a mean komatiitic composition. Most of the other rocks (e.g., m2) are located close to the early Skaergaard tholeiitic trend. In mantle-normalized plots (Fig. 10a, b), the rocks of site m2 (Fig. 5d) were compared with the Kasigau group amphibolite (Fig. 5b) and an amphibolite sample from the Galana River shear zone (Fig. 5a). Although different in absolute concentrations the enrichment patterns are similar and this

could, as in the Taita Hills-Galana River area, suggest a subduction influenced environment. Samples of m2 are different being enriched in the LREE (Figs. 5d, 10c). They may correspond to a within-plate setting as determined for Kurase group rocks. A close similarity can be found between cumulative rocks of m3 and those of m1 (rocks with lowest REE contents; Figs. 5c, e, 10d) implying that rocks of oceanic affinity may also be present at the latter site.

From a Th/La–Sm/La discrimination diagram (Fig. 10e) one can see that samples from m1 suggest an ocean island origin, but in the light of an arc-related setting, this could also indicate an OIB-like signature due to source heterogeneities that may be found in subduction environments (e.g., Gorrington and Kay 2001; Petrone et al. 2003). Also, the dissimilarity of the rocks of site m2 (Figs. 5d, 10a–c) are portrayed. Two samples, respectively, indicate a MORB to OIB- or a subduction setting (Fig. 10e). The rocks of m3 suggest arc crust after these criteria (Fig. 10e). As for the

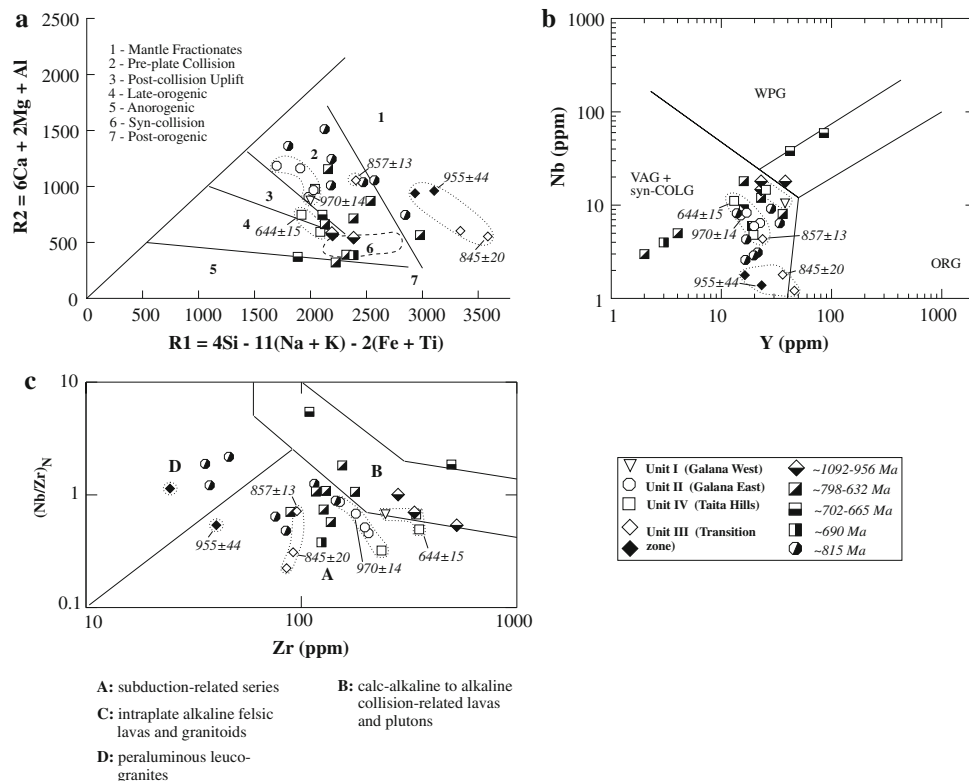


**Fig. 11** Tectonic setting **a** after Batchelor and Bowden (1985), **b** Pearce et al. (1984) and **c** Thiéblemont and Tegye (1994). Data from Kröner et al. (2003) Squares (half-filled diagonal and half-filled horizontal, Meso/Neoproterozoic model ages); Square half-filled vertical (granitic melt patch); Diamonds half-filled (Archean model ages). For clarity, the range of corresponding U/Pb ages (error margins: 0.7–0.9 Ma) are shown in the legend (see text for details).

data of SE Kenya it is worth mentioning that half of the samples plot in the MORB field (Fig. 10e). While some of the data of unit I and unit IV indicate an overlap to a MORB setting in previous plots (e.g., Figs. 8e, 9a, b) the samples from unit II solely suggested an arc-related source (Figs. 8e, f, 9a, b). A possible reason for lowered Th/La ratios (e.g., loss of Th, Fig. 2b) causing a shift of the data towards the MORB array could be the effects of granulite facies metamorphism (see Plank 2005 and references therein).

Summarizing the results, it is suggested that the data from the Pare mountains (and possibly also Usambara mountains) could indicate rifting, subduction and rocks of ophiolitic nature. In contrast, Prochaska and Pohl (1983) indicated a non-ophiolitic origin (derivation from subcontinental mantle) for a few mafic to ultramafic samples of the Pare mountains. This may be conformable to magmatic underplating (Appel et al. 1998), and which may account for such rocks. As, however, the model of the latter authors is based on the assumption of an active continental margin, the existing and new results are not inconsistent.

Circles half-filled as in Fig. 7. Dotted lines accentuate the data of this study. Dashed line in a array of syn-collisional granites. WPG within-plate granites; ORG ocean-ridge granites; VAG + syn-COLG volcanic arc- to syn-collisional granites. U/Pb age data (SE Kenya samples, Table 1; Fig. 1): 970 ± 14 Ma (KGB35LF); 955 ± 44 Ma (K209); 845 ± 20 Ma (K120); 857 ± 13 Ma (KGB174); 644 ± 15 Ma (K37)

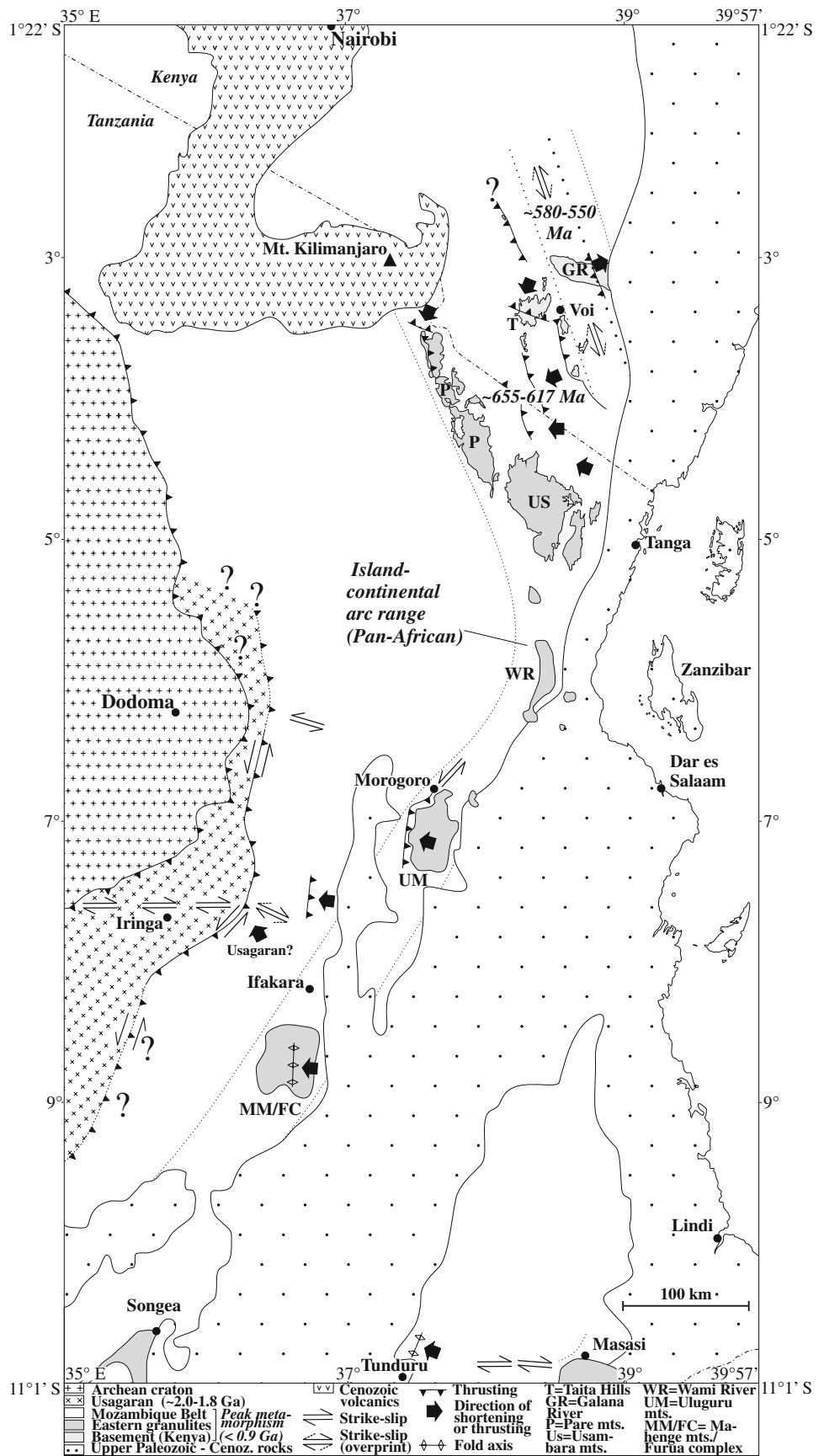
On the other hand, some of the rocks may show pre-Pan-African crust (see “Discussion”) and could be related to a different setting.

Gneisses (metagranitoids)

Study area

For a comparison ocean ridge granite-normalized graphs were used including data of well-known geotectonic settings (Pearce et al. 1984, Fig. 7e–g). In addition, a tectonic setting is determined using the multication diagram of Batchelor and Bowden (1985, Fig. 11a) as well as Y–Nb (Pearce et al. 1984, Fig. 11b) and Zr–(Nb/Zr)<sub>N</sub> plots (Thiéblemont and Tegye 1994; Thiéblemont 1999; Fig. 11c). As afore-mentioned, granitoid gneisses from the Usambara mountains (Maboko and Nakamura 2002) and SE Tanzania (Kröner et al. 2003) are shown together with our data (Figs. 11a–c). The Usambara samples (La ≈ 29–73× chondrite; La<sub>n</sub>/Lu<sub>n</sub> ≈ 3.2–6.7; Fig. 7d) are from a section from Mombo to Lushoto (Fig. 1). The rocks were

**Fig. 12** Simplified tectonic sketch (after Shackleton 1986; Muhongo and Lenoir 1994; Möller et al. 2000; Kröner et al. 2003; Hauzenberger et al. 2004; Bauernhofer 2003). *Shaded areas* basement rocks (SE Kenya) and eastern granulites (Tanzania). These areas, belonging to the Mozambique belt, indicate possible vestiges of a Pan-African island-continental arc range (the *dotted line* highlights the trend of the domain). Span of peak metamorphic ages: according to Appel et al. 1998; Möller et al. 2000; Muhongo et al. 2001; Hauzenberger et al. 2007. An intrusion age of ~580 Ma (syntectonic pegmatite) is assumed to relate to a high-grade event. *Bold dotted line* (Galana River area): eastern border of the Galana River shear zone (unit II). To the east of the Galana River shear zone, a late Pan-African granulite facies event (~550 Ma) was dated in unit I (Hauzenberger et al. 2007)



dated at  $815 \pm 58$  Ma (Sm–Nd whole rock dating), show Nd model ages of  $\sim 1.0$  to  $1.1$  Ga and were interpreted as juvenile addition of a convergent margin setting. The SE Tanzania samples (Masasi area; Fig. 12) show two groups of U–Pb zircon ages. Meso- to Neoproterozoic metaplutonic rocks ( $\sim 1.1$ – $0.96$  Ga, three samples) indicate Nd model ages of  $\sim 2.6$ – $2.7$  Ga and were interpreted as remelted Archean crust. Early to mid-Neoproterozoic intrusions ( $\sim 798$ – $632$  Ma, 10 samples), considered as juvenile melts, yield model ages of  $\sim 0.8$ – $1.25$  Ga.

The gneisses of the Galana River shear zone (unit II) and the Taita Hills (unit IV) suggest volcanic-arc resemblance as can be noted, e.g., in relation to granitoids of Chile and Jamaica (Fig. 7e, f). This setting could be true also for rocks of the Transition zone (unit III) which broadly differ in lower HFSE concentrations (Nb, Zr, Hf). The different position of these gneisses is shown in Fig. 11a in which the samples classify as mantle fractionates. A fractionated nature can also be noted from the criteria suggested by Whalen et al. (1987) (Fig. 6f). Another distinctive feature of these gneisses could be low  $K_2O/Na_2O$  ratios (Table 2), which are typical of island-arc granitoids. In the Y–Nb discrimination diagram (Fig. 11b), the samples of SE Kenya and the Usambara mountains define volcanic-arc to syncollisional rocks. According to the complementary Rb–(Y + Nb) graph (Pearce et al. 1984; not shown) they are of volcanic arc origin. This is supported by Fig. 11a, which indicates a pre-collisional setting except for two gneisses from unit IV. The latter suggest a late-tectonic to post-collisional origin (Fig. 11a). Zr–(Nb/Zr)<sub>N</sub> ratios (Fig. 11c) which are also a measure of contamination with older crust (Thiéblemont 1999, field B) indicate (Fig. 11a, b) a subduction related (pre-collisional) origin for the majority of the gneisses of SE Kenya and NE Tanzania. Four samples are a similarity to leucogranitoids.

#### *Metagneous rocks from SE Tanzania*

The data from SE Tanzania show a wider scatter (Fig. 11a–c). The older rocks (three samples,  $\sim 1.1$ – $0.96$  Ga) plot in Fig. 11a as late orogenic ( $\sim 1.0$ ,  $0.96$  Ga) and syn-collisional rocks ( $\sim 1.1$  Ga). The Y–Nb plot (Fig. 11b) shows a volcanic arc to syn-collisional origin (volcanic arc according to Rb–(Y + Nb) systematics) of two samples ( $\sim 1.1$ ,  $0.96$  Ga). The other sample ( $\sim 1.0$  Ga) indicates a within-plate source or (subject to Rb–(Y + Nb) ratios) overlaps the limit of within-plate and volcanic-arc granitoids. The Zr–(Nb/Zr)<sub>N</sub> discrimination (Fig. 11c) suggests a collisional related origin (two samples,  $\sim 1.1$ ,  $0.96$  Ga). One sample ( $\sim 1.0$  Ga) overlaps the limit of collisional and subduction-related sources.

The younger rocks (10 samples,  $\sim 798$ – $632$  Ma) (Fig. 11b) suggest both a volcanic arc-syn-collisional

[volcanic arc due to Rb–(Y + Nb) ratios] and a within-plate setting. The rocks belonging to the former setting (eight samples) define pre-collisional granitoids ( $\sim 798$ ,  $793$ , and  $676$  Ma) and mantle fractionates ( $\sim 767$  Ma) or indicate syn-collisional rocks ( $\sim 690$ ,  $632$  Ma) (Fig. 11a). One of the latter refers to a granitic melt patch ( $\sim 690$  Ma) and should be interpreted with caution. The remaining two samples overlap the limit of late/anorogenic origin ( $\sim 658$  Ma) or rather suggest post-collisional magmatism ( $\sim 739$  Ma). The samples defining a within-plate setting (Fig. 11b) straddle the fields of post/pre-plate collision ( $\sim 665$  Ma) or the array of late/anorogenic granitoids ( $\sim 702$  Ma) (Fig. 11a).

The Zr–(Nb/Zr)<sub>N</sub> classification (Fig. 11c) largely corresponds to the Y–Nb plot (Fig. 11b). The rocks which indicate within-plate origin (Fig. 11b) show separate positions whereas one sample ( $\sim 665$  Ma) implies such a setting. In this classification, rocks displayed as collision-related (pre-collisional in Fig. 11a) have intrusion ages of  $\sim 767$  Ma and  $\sim 793$  Ma.

## Discussion

### Problem and significance

The basement rocks of the study area were subjected to multiple deformation caused either by different events or an enduring event. This is supported by petrological studies (Hauzenberger et al. 2004; Appel et al., 1998; Möller et al. 2000) which show granulite facies events and subsequent retrogression of the rocks of the study area. Therefore fluid infiltration (element mobilities) may have occurred which geotectonic interpretations could put into perspective. However, considerable element mobility need not necessarily be the case in high-grade rocks as shown, e.g., by Rockow et al. (1997). For a change from granulite to eclogite facies conditions, the authors detected no significant gain or loss of elements unless the overprint was connected with distinct shear domains.

Other studies generally emphasize the problem of geotectonic interpretations of lower crustal rocks (e.g., Condie et al. 2004). Due to the often complex history of such rocks, whole rock ratios (HFSE or REE) may have no clear significance in terms of a tectonic setting. Another fundamental problem concerns the geochemical signatures themselves. They may reflect precursor rocks rather than being characteristic of rocks evolved from a subsequent tectonic setting. This was suggested, e.g., for calc-alkaline I-type granitoids showing high-K content (Roberts and Clemens 1993). In the present case, most metaplutonic rocks of SE Tanzania (ten samples) as well as three gneiss samples of SE Kenya have high-K content. Although this



may be due to element mobility or metasomatism, in the context of orogenic events such granitoids occur in continental arcs or post-collisional settings. Similarly, heterogeneous oceanic crust could bias geochemical patterns of subduction-related mafic to ultramafic rocks. In addition to MORB, subducted oceanic crust may contain a variety of mafic rock types (e.g., Spandler et al. 2004). Thus different geochemical patterns could partly represent a single piece of subducted crust. Lastly, also the architecture of ophiolitic crust may complicate the interpretation (e.g., Moores 2002). The characteristic compositions of ophiolites may vary through time and obducted remnants occasionally contain rocks with geochemical signatures similar to subduction zones.

Notwithstanding these problems, we believe that there is sufficiently reliable evidence to infer a geotectonic setting. The results of major and trace element discrimination plots coincide and (in combination with trace element ratios; Table 2) show a close similarity to data of well-known settings. In addition, rocks of similar geochemical affinity were often located in specific structural domains (e.g., thrust or strike slip dominated) or indicate a different metasedimentary background (e.g., Kurase and Kasigau group; Saggerson 1962; Pohl et al. 1980). This argues for the significance of the data and that the domains might mark particular geotectonic positions, either of a continuous system (continental or island arc) or of different origin (continental and island arc domains, e.g., Japan, New Zealand) or different arc types.

#### Implications for Pan-African subduction and collision

For several reasons, the interpretation of orthogneisses may be important. On the one hand, mafic rocks which may relate to subduction or rifting were not dated. Hence connections to Pan-African magmatism rely on gneiss protoliths. On the other hand, rocks of unit III show similarities to island arc granitoids and may indicate such a setting in contact (or in addition) to a continental arc. Recent dating (Hauzenberger et al. 2007) shows the intrusion of metagranitoids from unit III at ~955–845 Ma. Nd model ages derived from two of these metagranitoids indicate a pre-Pan-African crustal component (~1.4, 1.8 Ga) and implies emplacement into pre-Pan-African basement or a genetic interaction with older rocks. Although the two metagranitoid samples have high  $^{147}\text{Sm}/^{144}\text{Nd}$  ratios ( $\geq 0.17$ ) which could query calculated Nd model ages (e.g., Möller et al. 1998; Stern 2002), zircon xenocrysts (~1.4 Ga; one sample) support the idea that there is a contamination with older crust.

In addition to pre-collisional metagranitoids (the youngest age is from the northern part of unit IV, Fig. 1), two data from the upper Kurase group in unit IV (Fig. 1)

suggest a late-tectonic to post-collisional origin (Fig. 11a). This is also supported by zircon data. The sample beneath the Wanjala thrust (Fig. 1) yields an age of ~644 Ma and is considered to represent syn-metamorphic emplacement rather than a metamorphic age (Hauzenberger et al. 2007). A syn- to late-tectonic origin for the rocks is also indicated by their gneissic fabric. Thus the indicated setting would coincide with the early phase of Pan-African granulite facies associated with a Pan-African suture proposed to run through the Taita Hills (Frisch and Pohl 1986). In this setting, the importance of the Galana River area is not clear. Notably, this concerns the eastern Galana River (unit I) where emplacement ages for gneisses have not been determined. The younger granulite facies metamorphism (~550 Ma) may reflect a separate event or cycle in Gondwana amalgamation. The more metasedimentary character of unit I (Sanders 1963) could also point to a different terrane but, in part, of island to continental arc composition.

In NE Tanzania granulite facies metamorphism took place between ~655 and 617 Ma (e.g., Möller et al. 2000; Muhongo and Lenoir 1994), corresponding to the older Pan-African peak metamorphism in SE Kenya. Other similarities between the two areas are indicated by igneous ages and geochemical data. Muhongo et al. (2001) deduced Pan-African intrusion ages of ~754 and ~656 Ma from gneisses of the eastern Usambara Mountains (Fig. 1). Geochemical data from the Usambara mountains (Maboko and Nakamura 2002) support a subduction setting and display low HFS element concentrations, similar to the gneisses of unit III (Fig. 7g, h). A convergent setting also follows from data of Appel (1996) who noticed a subduction origin for enderbite rocks from the Pare-Usambara- and Uluguru mountains (Fig. 12). Recent data (Tenczer et al. 2006) suggest that this setting may have existed since the early Neoproterozoic in the Uluguru- and possibly also in the Mahenge mountains (Fig. 12).

The data from SE Tanzania (Kröner et al. 2003) demonstrate a complex geological setting, including evidence for early- to mid-Neoproterozoic subduction- to collision-related rocks. The rocks which suggest intraplate conditions (~702–665 Ma) are most striking. Based on two samples this setting is ambiguous. However, the authors noticed a high-grade melting event (<700 Ma) in relation to late terrane assembly. Another feature includes late Mesoproterozoic to early Neoproterozoic (~1.1–0.96 Ga) calc-alkaline rocks derived from Archean basement. In discrimination plots they straddle, in part, several fields (Figs. 10a–c) and probably form tectonic inliers into the younger basement. Although speculative, the lower age may already involve early Pan-African convergence as suggested for SE Kenya.

### Implications for Pan-African rifting

If the rift-related rocks of the Taita Hills play a role in a Pan-African setting they may reflect a continental rifting or, solely linked to Pan-African convergence, back-arc rifting. This setting could also apply to rocks of the Pare Mountains (e.g., site m2). There, both sources appear to be interrelated and may allude to incipient back-arc formation as reported, e.g., from the northwestern Pacific (e.g., Ikeda and Yuasa 1989). Thus, rocks of site m1–m3 (Fig. 1) may reflect portions of arc- to back-arc crust.

As in SE Kenya, the relevance of mafic- to ultramafic rocks of the Pare Mountains for the Pan-African cycle is uncertain. Dundas (1965) suggested a common origin of the Ikongwe meta-anorthosite (Fig. 1) categorized as Adirondack type and ultrabasic bodies, and noticed a resemblance to the Uluguru mountains meta-anorthosite (see Muhongo and Lenoir 1994; Tenczer et al. 2006). Tenczer et al. (2006) showed emplacement ages of  $\sim 2.64$  Ga for the meta-anorthosite of Ikongwe and accordingly  $\sim 880$ – $820$  Ma for the Uluguru mountains meta-anorthosite. The former result may have consequences on the geotectonic interpretation. If the suggestion of Dundas (1965) is correct, some of the mafic- to ultramafic rocks (Pare-Usambara Mountains, Uмба Steppe) could also be much older. Then rocks of site m2 (nearby Ikongwe; Fig. 1) may be vestiges of an older cycle (e.g., (pre)-Usagaran). On the other hand, the meta-anorthosite from the Uluguru Mountains is linked with a Pan-African event. Metamorphic overprints occurred at  $\sim 695$  Ma (Muhongo and Lenoir 1994) and  $\sim 640$ – $650$  Ma (Tenczer et al. 2006). For the rocks, Muhongo and Lenoir (1994) suggested the emplacement into a Pan-African subduction-collisional environment. Gibson and Ireland (1999) proposed a magmatic arc setting inducing rifting and back-arc extension for a Paleozoic anorthosite from New Zealand. They noticed a resemblance to the Andean arc (see also references therein) and discussed a similar origin for Archean equivalents. An arc related rift was also considered for the Uluguru mountains meta-anorthosite (Tenczer et al. 2006). This argument was based on different ages derived from the meta-anorthosite ( $\sim 880$ – $820$  Ma) and calc-alkaline host gneiss ( $\sim 986$  Ma). Consequently, a convergent tectonic setting is plausible for the rocks of the Uluguru Mountains. Anorthosite bodies are also found to the NNW of the Taita Hills-Galana River area in central eastern Kenya (see Mosley 1993). Likewise, some of these rocks may be connected with a magmatic arc setting.

### Implications for the Pan-African cycle

Considering the Mozambique belt within a global tectonic framework the rift related rocks of the study area may

reflect incipient Rodinia breakup ( $\geq 1.0$  Ga). Thus, early subduction could signify an area at the margin of the supercontinent. By contrast, the rocks could be part of a Pan-African volcanic arc setting ( $\leq 1.0$  Ga) which may, but need not, result from the disintegration of the supercontinent. This relationship is also important for the southern portions of the eastern granulites in Tanzania (Fig. 12).

The early onset of Pan-African orogenesis was reported from the Tocantins province in central Brazil (e.g., Pimentel and Fuck 1992). There, island arc formation started at about  $\sim 900$  Ma and proceeded as arc-type magmatism up to the Brasiliano orogeny ( $\sim 600$  Ma). Younger Pan-African magmatism was reported, e.g., from the southern Arabian Nubian Shield (Ethiopia) where early arc-related granitoids have  $\sim 850$ – $770$  Ma ages (e.g., Tadesse et al. 2000; Ayalew and Peccerillo 1998; Teklay et al. 1998; Johnson et al. 2004).

### Conclusions

Taking into account the limitations discussed above, the following conclusions may be drawn: Amphibolitic rocks from the Taita Hills-Galana River area suggest a volcanic arc setting. An appreciable subduction component is indicated for rocks of the Galana River shear zone (unit II), while a more MORB-like source (or rather decreasing subduction influence) dominates in the western and central area of unit I. In the eastern area of unit I, characteristic LIL- and HFS element concentrations again appear to reflect subduction-related processes. In SE Kenya a change from rifting to subduction was previously suggested (Frisch and Pohl 1986). Overall, the new results reinforce this opinion and suggest that the Kasigau- and Kurase group may interrelate as a Pan-African volcanic arc/back-arc system. Such a setting is also consistent with rocks of NE Tanzania, although age relations are more speculative. In addition, ophiolitic remnants may be preserved. Some of the mafic to ultramafic rocks could form tectonized portions of differentiation sequences as can be seen, e.g., from REE patterns. The investigated gneisses from SE Kenya support a volcanic-arc setting. Gneisses from unit III could signify former metagranitoids which were generated due to subduction of an oceanic slab.

The occurrence of early Pan-African island (continental)-arc material is comparable to settings of the Arabian-Nubian Shield (see also Maboko and Nakamura 2002), where arc-arc- to arc-continental sutures formed between  $\sim 830$  and  $\sim 620$  Ma (e.g., Abdelsalam and Stern 1996; Johnson and Woldehaimanot 2003; Whitehouse et al. 2001). This suggests a southward continuation of such arc sequences from the ANS into the central Mozambique

Belt (Fig. 12) where crust formation, in part, may have started earlier. Thus the study area records development of an arc with incipient convergence (island to continental arc formation) and continental or back-arc rifting, followed by accretion [arc-continental (arc)] and continent–continent collision during a long-lived continuous or multiple, separate convergent cycles.

**Acknowledgments** We would like to thank our colleagues from the University of Nairobi and Dar es Salaam who have supported this work. Sincere thanks are given to T. Schlüter and D. Hollnack for their help, E. M. Mathu for support in the field and G. Niedermayr for providing maps and reports from SE Kenya. Many thanks to the rangers of the Tsavo East National Park, J. Loizenbauer and H. Fritz for discussion and that they brought along a gneiss sample from the western Galana area, and to F. Bernhard for his help to start the work and valuable comments. A.B. is much indebted to Peter R. Johnson and Victoria Pease for thorough reviews of the ms which greatly improved the readability, presentation and evaluation of the data. The final version was again refined by numerous corrections and suggestions of V. Pease. The fundamental criticism and specific comments by Kent Condie on an earlier version are greatly acknowledged. W. Pohl is thanked for a discussion several years ago (that was not necessarily focused on geology) as well as W. Piller who provided working facilities. I am further indebted to topic editor R. J. Stern and editor W.-Chr. Dullo that this data and ideas could be presented in an international journal. This study was made possible by funding from the Austrian Science Foundation (FWF grants P12375-GEO and P15599) which also allowed me and colleagues to undertake several field trips to E Africa.

## References

- Abdelsalam M, Stern RJ (1996) Sutures and shear zones in the Arabian–Nubian Shield. *J Afr Earth Sci* 23:289–310. doi: [10.1016/S0899-5362\(97\)00003-1](https://doi.org/10.1016/S0899-5362(97)00003-1)
- Appel P, Möller A, Schenk V (1998) High-pressure granulite facies metamorphism in the Pan-African Belt of eastern Tanzania: P-T-t evidence against granulite formation by continent collision. *J Metamorph Geol* 16:491–509. doi: [10.1111/j.1525-1314.1998.00150.x](https://doi.org/10.1111/j.1525-1314.1998.00150.x)
- Appel P (1996) Hochdruckgranulite und Eklogite im Mozambique Belt von Tansania: eine geochemische und petrologische Studie. Dissertation, Christian-Abrechts-Universität Kiel, Deutschland
- Ayalew T, Peccerillo A (1998) Petrology and geochemistry of the Gore-Gambella plutonic rocks; implications for magma genesis and the tectonic setting of the Pan-African orogenic belt of western Ethiopia. *J Afr Earth Sci* 27:397–416. doi: [10.1016/S0899-5362\(98\)00070-0](https://doi.org/10.1016/S0899-5362(98)00070-0)
- Bagnall PS (1960) The geology of the north Pare Mountains. *Rec Geol Surv Tanganyika* 10:7–16
- Bagnall PS, Dundas D, Hartley E (1963) Geological map of the Usambara Mountains (Lushoto), scale 1:125,000. Geological Survey Divison, Dodoma, Tanganyika
- Basaltic Volcanism Study Project (1981) Basaltic volcanism on the terrestrial planets. Pergamon Press, New York, pp 236–281
- Batchelor RA, Bowden P (1985) Petrological interpretation of granitoid rock series using multicationic parameters. *Chem Geol* 48:43–55. doi: [10.1016/0009-2541\(85\)90034-8](https://doi.org/10.1016/0009-2541(85)90034-8)
- Bauernhofer AH (2003) Tectonic setting of early- to late Pan-African structures from the Mozambique Belt in SE Kenya and NE Tanzania. PhD Thesis, Karl-Franzens-Universität Graz, Austria
- Berhe SM (1990) Ophiolites in northeast and east Africa: implications for Pan-African crustal growth. *J Geol Soc Lond* 147:41–57. doi: [10.1144/gsjgs.147.1.0041](https://doi.org/10.1144/gsjgs.147.1.0041)
- Boynton WV (1984) Cosmochemistry of rare earth elements; meteorite studies. In: Henderson P (ed) Rare earth element geochemistry. Elsevier, Amsterdam
- Chappell BW, White AJR (1974) Two contrasting granite types. *Pac Geol* 8:173–174
- Coleman RG (1977) Ophiolites; ancient oceanic lithosphere?. Springer, Berlin, pp 1–229
- Condie KC, Cox J, O'Reilly SY, Griffin WL, Kerrich R (2004) Distribution of high field strength and rare earth elements in mantle and lower crustal xenoliths from the southwestern United States: the role of grain-boundary phases. *Geochim Cosmochim Acta* 68:3919–3942. doi: [10.1016/j.gca.2004.03.025](https://doi.org/10.1016/j.gca.2004.03.025)
- Coolen JJMM, Priem HMA, Verdurmen EAT, Verschure RH (1982) Possible zircon U–Pb evidence for Pan-African granulite-facies metamorphism in the Mozambique Belt of southern Tanzania. *Precambrian Res* 17:31–40. doi: [10.1016/0301-9268\(82\)90152-8](https://doi.org/10.1016/0301-9268(82)90152-8)
- Debon F, Le Fort B (1983) A chemical–mineralogical classification of common plutonic rocks and associations. *Trans R Soc Edinb Earth Sci* 73:135–149
- Dilek Y, Thy P (2006) Age and petrogenesis of plagiogranite intrusions in the Ankara mélange, central Turkey. *Isl Arc* 15:44–57. doi: [10.1111/j.1440-1738.2006.00522.x](https://doi.org/10.1111/j.1440-1738.2006.00522.x)
- D'Orazio M, Innocenti F, Manetti P, Haller MJ (2004) Cenozoic back-arc magmatism of the southern extra-Andean Patagonia (44°30'–52°S): a review of geochemical data and geodynamic interpretations. *Rev Assoc Geol Argent* 59:525–538
- Dundas L (1965) Geological map of the South Pare mountains (Same), scale 1:125 000. Geological Survey Divison, Dodoma, Tanganyika
- Farquhar OC (1960) Geology and asbestos deposits of the Taita Hills, Kenya. *Mem Geol Surv Kenya* 2:1–110
- Frisch W, Pohl W (1986) Petrochemistry of some mafic and ultramafic rocks from the Mozambique Belt, SE Kenya. *Mitt österr Geol Ges* 78:97–114
- Gamble JA, Smith IEM, McCulloch MT, Graham IJ, Kokelaar BP (1993) The Geochemistry and petrogenesis of basalts from the Taupo volcanic zone and Kermadec island arc, SW Pacific. *J Volcanol Geotherm Res* 54:265–290. doi: [10.1016/0377-0273\(93\)90067-2](https://doi.org/10.1016/0377-0273(93)90067-2)
- Gamble JA, Wright IC, Woodhead JD, McCulloch MT (1995) Arc and back-arc geochemistry in southern Kermadec arc–Ngatoro Basin and offshore Taupo Volcanic Zone, SW Pacific. In: Smellie JL (ed). *Volcanism associated with extension at consuming plate margins*. *Geol Soc Spec Publ* 81:193–212
- Gibson GM, Ireland TR (1999) Black Giants Anorthosite, New Zealand: a Paleozoic analogue of Archean stratiform anorthosites and implications for the formation of Archean high-grade gneiss terranes. *Geology* 27:131–134. doi: [10.1130/0091-7613\(1999\)027<0131:BGANZA>2.3.CO;2](https://doi.org/10.1130/0091-7613(1999)027<0131:BGANZA>2.3.CO;2)
- Gill J (1981) Orogenic andesites and plate tectonics. Springer, Berlin, pp 1–390
- Gorring ML, Kay SM (2001) Mantle processes and sources of neogene slab window magmas from Southern Patagonia, Argentina. *J Petrol* 42:1067–1094. doi: [10.1093/petrology/42.6.1067](https://doi.org/10.1093/petrology/42.6.1067)
- Hartley E, Moore W (1965) Quarter degree sheet 91, 110 (Daluni), scale 1:125,000. Geological Survey Divison, Dodoma
- Hauzenberger CA, Sommer S, Fritz H, Bauernhofer A, Kröner A, Hoinkes G et al (2007) SHRIMP U–Pb zircon and Sm–Nd garnet ages from granulite facies basement of SE-Kenya: evidence for Neoproterozoic polycyclic assembly of the Mozambique belt. *J Geol Soc Lond* 164:189–201. doi: [10.1144/0016-76492005-081](https://doi.org/10.1144/0016-76492005-081)
- Hauzenberger CA, Bauernhofer AH, Hoinkes G, Wallbrecher E, Mathu EM (2004) Pan-African high pressure granulites from SE



- Kenya: petrological and geothermobarometric evidence for a polycyclic evolution in the Mozambique belt. *J Afr Earth Sci* 40:245–268. doi:[10.1016/j.jafrearsci.2004.12.004](https://doi.org/10.1016/j.jafrearsci.2004.12.004)
- Haraguchi S, Ishii T, Kimura J-I, Ohara Y (2003) Formation of tonalite from basaltic magma at the Komahashi-Daini Seamount, northern Kyushu-Palau Ridge in the Philippine Sea, and growth of Izu-Ogasawara (Bonin)-Mariana arc crust. *Contrib Mineral Petrol* 145:151–168
- Horkel A, Niedermayr G, Wachira JK, Pohl W, Okelo REA, Nauta WJ (1979) Geology of the Taita Hills. *Rep Geol Surv Kenya* 102:1–33
- Ikeda Y, Yuasa M (1989) Volcanism in nascent back-arc basins behind the Shichito Ridge and adjacent areas in the Izu-Ogasawara arc, northwest Pacific: evidence for mixing between E-type MORB and island arc magmas at the initiation of back-arc rifting. *Contrib Mineral Petrol* 101:377–393. doi:[10.1007/BF00372212](https://doi.org/10.1007/BF00372212)
- Johnson TE, Ayalew T, Mogessie A, Kruger FJ, Poujol M (2004) Constraints on the tectonometamorphic evolution of the Western Ethiopian Shield. *Precambrian Res* 133:305–327. doi:[10.1016/j.precamres.2004.05.007](https://doi.org/10.1016/j.precamres.2004.05.007)
- Johnson PR, Woldehaimanot B (2003) Development of the Arabian-Nubian Shield; perspectives on accretion and deformation in the northern East African Orogen and the assembly of Gondwana. *Geol Soc Spec Publ* 206:289–325
- Johnson SP, Cutton HNC, Muhongo S, De Waele B (2003) Neoproterozoic magmatism and metamorphism of the western granulites in the central domain of the Mozambique Belt, Tanzania: U-Pb SHRIMP geochronology and PT estimates. *Tectonophysics* 325:125–145. doi:[10.1016/j.tecto.2003.06.003](https://doi.org/10.1016/j.tecto.2003.06.003)
- Key RM, Charsley TJ, Hackman BD, Wilkinson AF, Rundle CC (1989) Superimposed Upper Proterozoic Collision-controlled Orogenies in the Mozambique Orogenic Belt of Kenya. *Precambrian Res* 44:197–225. doi:[10.1016/0301-9268\(89\)90045-4](https://doi.org/10.1016/0301-9268(89)90045-4)
- Klein EM, Langmuir CH, Staudigel H (1991) Geochemistry of basalts from the Southeast Indian Ridge, 115°E–138°. *J Geophys Res* 92:8089–8115. doi:[10.1029/JB092iB08p08089](https://doi.org/10.1029/JB092iB08p08089)
- Knittel U, Oles D (1995) Basaltic volcanism associated with extensional tectonics in the Taiwan-Luzon island arc: evidence for non-depleted sources and subduction zone enrichment. In Smellie JL (ed) *Volcanism associated with extension at consuming plate margins*. *Geol Soc Spec Publ* 81:77–93
- Koepke J, Feig ST, Snow J, Freise M (2004) Petrogenesis of oceanic plagiogranites by partial melting of gabbros: an experimental study. *Contrib Mineral Petrol* 146:414–432. doi:[10.1007/s00410-003-0511-9](https://doi.org/10.1007/s00410-003-0511-9)
- Kröner A, Muhongo S, Hegner E, Wingate MTD (2003) Single zircon geochronology and Nd isotopic systematics of Proterozoic high-grade rocks from the Mozambique belt of southern Tanzania (Masasi area): implications for Gondwana assembly. *J Geol Soc Lond* 160:745–757. doi:[10.1144/0016-764901-170](https://doi.org/10.1144/0016-764901-170)
- Le Bas MJ, Le Maitre RW, Streckeisen A, Zanettin BA (1986) Chemical classification of volcanic rocks based on the total alkali-silica diagram. *J Petrol* 27:745–750
- Leake BE (1964) The chemical distinction between ortho- and para-amphibolites. *J Petrol* 5:238–254
- Lentz DR (1998) Petrogenetic evolution of felsic volcanic sequences associated with Phanerozoic volcanic-hosted massive sulphide systems: the role of extensional geodynamics. *Ore Geol Rev* 12:289–327. doi:[10.1016/S0169-1368\(98\)00005-5](https://doi.org/10.1016/S0169-1368(98)00005-5)
- Maboko MAH, Nakamura E (2002) Isotopic dating of Neoproterozoic crustal growth in the Usambara Mountains of northeastern Tanzania: evidence for coeval crust formation in the Mozambique Belt and the Arabian-Nubian Shield. *Precambrian Res* 113:227–242. doi:[10.1016/S0301-9268\(01\)00213-3](https://doi.org/10.1016/S0301-9268(01)00213-3)
- Mercier A, Debat P, Saul JM (1999) Exotic origin of the ruby deposits of the Mangari area in SE Kenya. *Ore Geol Rev* 14:83–104. doi:[10.1016/S0169-1368\(99\)00002-5](https://doi.org/10.1016/S0169-1368(99)00002-5)
- Möller A, Mezger K, Schenk V (1998) Crustal Age domains and the Evolution of Continental Crust in the Mozambique Belt of Tanzania. Combined Sm-Nd, Rb-Sr, Pb-Pb Isotopic Evidence. *J Petrol* 39:749–783
- Möller A, Mezger K, Schenk V (2000) U–Pb dating of metamorphic minerals: Pan-African metamorphism and prolonged slow cooling of high-pressure granulites in Tanzania, East Africa. *Precambrian Res* 104:123–146. doi:[10.1016/S0301-9268\(00\)00086-3](https://doi.org/10.1016/S0301-9268(00)00086-3)
- Moore EM (2002) Pre-1 Ga (pre-Rodinia) ophiolites: their tectonic and environmental implications. *Geol Soc Am Bull* 114:80–95. doi:[10.1130/0016-7606\(2002\)114<0080:PGPROT>2.0.CO;2](https://doi.org/10.1130/0016-7606(2002)114<0080:PGPROT>2.0.CO;2)
- Mosley PN (1993) Geological evolution of the late Proterozoic “Mozambique Belt” of Kenya. *Tectonophysics* 221:223–250. doi:[10.1016/0040-1951\(93\)90334-G](https://doi.org/10.1016/0040-1951(93)90334-G)
- Muhongo S, Lenoir JL (1994) Pan-African granulite-facies metamorphism in the Mozambique Belt of Tanzania: U–Pb zircon geochronology. *J Geol Soc Lond* 151:343–347. doi:[10.1144/gsjgs.151.2.0343](https://doi.org/10.1144/gsjgs.151.2.0343)
- Muhongo S, Kröner A, Nemchin AA (2001) Single Zircon evaporation and SHRIMP ages for Granulite-Facies rocks in the Mozambique belt of Tanzania. *J Geol* 109:171–189. doi:[10.1086/319240](https://doi.org/10.1086/319240)
- Parkinson J (1947) *Outlines of the Geology of the Mtito Andei-Tsavo area, Kenya Colony*. *Rep Geol Surv* 13:1–40
- Pearce JA (1982) Trace element characteristics of lavas from destructive plate boundaries. In: Thorpe RS (ed) *Andesites; orogenic andesites and related rocks*. Wiley, Chichester
- Pearce JA, Harris NBW, Tindle AG (1984) Trace element discrimination diagrams for the tectonic interpretation of granitic rocks. *J Petrol* 25:956–983
- Petrone CM, Francalanci L, Carlson RW, Ferrari L, Conticelli (2003) Unusual coexistence of subduction-related and intraplate-type magmatism: Sr, Nd and Pb isotope and trace element data from the magmatism of the San Pedro-Ceboruco graben (Nayarit, Mexico). *Chem Geol* 193:1–24. doi:[10.1016/S0009-2541\(02\)00229-2](https://doi.org/10.1016/S0009-2541(02)00229-2)
- Piercey SJ, Murphy DC, Mortensen JK, Creaser RA (2004) Mid-Paleozoic initiation of the northern Cordilleran marginal backarc basin: Geologic, geochemical, and neodymium isotope evidence from the oldest mafic magmatic rocks in the Yukon-Tana terrane, Finlayson Lake district, southeast Yukon, Canada. *Geol Soc Am Bull* 116:1087–1106. doi:[10.1130/B25162.1](https://doi.org/10.1130/B25162.1)
- Pimentel MM, Fuck AR (1992) Neoproterozoic crustal accretion in central Brazil. *Geology* 20:375–379. doi:[10.1130/0091-7613\(1992\)020<0375:NCAICB>2.3.CO;2](https://doi.org/10.1130/0091-7613(1992)020<0375:NCAICB>2.3.CO;2)
- Plank T (2005) Constraints from Thorium/Lanthanum on sediment recycling at subduction zones and the evolution of the continents. *J Petrol* 46:921–944. doi:[10.1093/petrology/egi005](https://doi.org/10.1093/petrology/egi005)
- Pohl W, Horkel A, Neubauer W, Niedermayr G, Okelo RE, Wachira JK, Werneck W (1980) Notes on the geology and mineral resources of the Mtito Andei-Taita area (southern Kenya). *Mitt österr geol Ges* 73:145–152
- Pohl W, Niedermayr G (1979) Geology of the Mwatate Quadrangle and the Vanadium Grossularite Deposits of the area. *Rep Geol Surv Kenya* 101:1–55
- Polat A, Hofmann AW, Münker CM, Regelous M, Appel PWU (2003) Contrasting geochemical patterns in the 3.7–3.8 Ga pillow basalt cores and rims, Isua greenstone belt, Southwest Greenland: Implications for postmagmatic alteration processes. *Geochim Cosmochim Acta* 67:441–457. doi:[10.1016/S0016-7037\(02\)01094-3](https://doi.org/10.1016/S0016-7037(02)01094-3)
- Prochaska W, Pohl W (1983) Petrochemistry of some mafic and ultramafic rocks from the Mozambique Belt, northern Tanzania. *J Afr Earth Sci* 1:183–191
- Roberts MP, Clemens JD (1993) Origin of high-potassium, calc-alkaline, I-type granitoids. *Geology* 21:825–828. doi:[10.1130/0091-7613\(1993\)021<0825:OOHPTA>2.3.CO;2](https://doi.org/10.1130/0091-7613(1993)021<0825:OOHPTA>2.3.CO;2)

- Rockow KM, Haskin LA, Jolliff BL, Fountain DM (1997) Constraints on element mobility associated with the conversion of granulite to eclogite along fractures in an anorthositic complex on Holsnøy, Norway. *J Metamorphic Geol* 15:401–418
- Rudnick RL, McLennan SM, Taylor SR (1985) Large ion lithophile elements in rocks from high-pressure granulite facies terrains. *Geochim Cosmochim Acta* 49:1645–1655. doi:10.1016/0016-7037(85)90268-6
- Saggerson EP (1962) Geology of the Kurase-Kasigau area. *Rep Geol Surv Kenya* 51:1–60
- Sanders LD (1963) Geology of the Voi-South Yatta Area. *Rep Geol Surv Kenya* 54:1–48
- Shand SJ (1927) Eruptive rocks. Their genesis, composition, classification and their relation to ore deposits. Murby, London
- Shackleton RM (1986) Precambrian collision tectonics in Africa. In: Coward MP, Ries AC (eds) *Collision tectonics*. Geological Society of London Spec Publ, vol 19, pp 329–349
- Shackleton RM (1993) Tectonics of the lower crust: a view from the Usambara Mountains, NE Tanzania. *J Struct Geol* 15:663–671. doi:10.1016/0191-8141(93)90154-3
- Shaw DW (1968) A review of the K–Rb fraction trends by covariance analysis. *Geochim Cosmochim Acta* 32:573–601. doi:10.1016/0016-7037(68)90050-1
- Spandler C, Hermann J, Arculus R, Mavrogenes J (2004) Geochemical heterogeneity and element mobility in deeply subducted crust; insights from high-pressure mafic rocks from New Caledonia. *Chem Geol* 206:21–42. doi:10.1016/j.chemgeo.2004.01.006
- Solesbury FW (1967) Gem corundum pegmatites in NE Tanganyika. *Econ Geol* 62:983–991
- Sommer H, Kröner A, Hauzenberger CA, Muhongo S, Wingate MTD (2003) Metamorphic petrology and zircon geochronology of high-grade rocks from the central Mozambique Belt of Tanzania: crustal recycling of Archean and Paleoproterozoic material during the Pan-African orogeny. *J Metamorph Geol* 21:915–934
- Stephenson NCN (2000) Geochemistry of granulite-facies granitic rocks from Battye Glacier, northern Prince Charles Mountains, East Antarctica. *Aust J Earth Sci* 47:83–94. doi:10.1046/j.1440-0952.2000.00762.x
- Stern RJ (2002) Crustal evolution in the East African Orogen: a neodymium isotopic perspective. *J Afr Earth Sci* 34:109–117. doi:10.1016/S0899-5362(02)00012-X
- Sun SS, McDonough WF (1989) Chemical and isotopic systematics of oceanic basalts; implications for mantle composition and processes. In: Saunders AD, Norry MJ (eds) *Magmatism in the ocean basins*. *Geol Soc Spec Publ*, vol 42, pp 313–345
- Tadesse T, Hoshino M, Suzuki K, Iizumi S (2000) Sm–Nd, Rb–Sr and Th–U–Pb zircon ages of syn- to post-tectonic granitoids from the Axum area of northern Ethiopia. *J Afr Earth Sci* 30:313–327. doi:10.1016/S0899-5362(00)00022-1
- Tarney J (1977) Petrology, mineralogy, and geochemistry of the Falkland Plateau basement rocks, Site 330, Deep Sea Drilling Project. Initial Reports of the Deep Sea Drilling Project 36, Ushuaia, Argentina to Rio de Janeiro, Brazil, April–May 1974, pp 893–921
- Taylor RN, Nesbitt RW (1998) Isotopic characteristics of subduction fluids in an intra-oceanic setting, Izu-Bonin Arc, Japan. *Earth Planet Sci Lett* 164:79–98. doi:10.1016/S0012-821X(98)00182-4
- Teklay M, Kröner A, Mezger K, Oberhänsli R (1998) Geochemistry, Pb–Pb single zircon ages and Nd–Sr isotope composition of Precambrian rocks from southern and eastern Ethiopia; implications for crustal evolution in East Africa. *J Afr Earth Sci* 26:207–227. doi:10.1016/S0899-5362(98)00006-2
- Tenczer V, Hauzenberger C, Fritz H, Whitehouse MJ, Mogessie A, Wallbrecher E et al (2006) Anorthosites in the Eastern Granulites of Tanzania—New SIMS zircon U–Pb age data, petrography and geochemistry. *Precambrian Res* 148:85–114. doi:10.1016/j.precamres.2006.03.004
- Thiéblemont D, Tegye M (1994) Geochemical discrimination of differentiated magmatic rocks attesting for the variable origin and tectonic setting of calc-alkaline magmas. *Sci Terre Planet* 319:87–94
- Thiéblemont D (1999) Discrimination between mantle- and crustal-derived Andean calc-alkaline lavas. *Sci Terre Planet* 329:243–250
- Whalen JB (1985) Geochemistry of an island-arc plutonic suite: the Uasilau-Yau Yau intrusive complex, New Britain, P.N.G. *J Petrol* 26:603–632
- Whalen JB, Currie KL, Chappell BW (1987) A-type granites; geochemical characteristics, discrimination and petrogenesis. *Contr Min Petrol* 95:407–419. doi:10.1007/BF00402202
- Whitehouse MJ, Windley BF, Stoesser DB, Al-Khirbash S, Ba-Bttat MAO, Haider A (2001) Precambrian basement character of Yemen and correlations with Saudi Arabia and Somalia. *Precambrian Res* 105:357–369. doi:10.1016/S0301-9268(00)00120-0
- Winchester JA, Floyd PA (1977) Geochemical discrimination of different magma series and their differentiation products using immobile elements. *Chem Geol* 20:325–343. doi:10.1016/0009-2541(77)90057-2
- Winchester JA, Park RG, Holland JG (1980) The geochemistry of Lewisian semipelitic schists from the Gairloch District, Wester Ross, North-West Scotland. *Scott J Geol* 16:165–179
- Wood DA (1980) The application of a Th–Hf–Ta diagram to problems of tectonomagmatic classification and to establishing the nature of crustal contamination of basaltic lavas of the British Tertiary volcanic province. *Earth Planet Sci Lett* 50:11–30. doi:10.1016/0012-821X(80)90116-8
- Woodhead J, Eggins S, Gamble J (1993) High field strength and transition element systematics in island arc and back-arc basin basalts: evidence for multi-phase melt. *Earth Planet Sci Lett* 114:491–504. doi:10.1016/0012-821X(93)90078-N